Title: Bidirectional Long-Term Synaptic Zinc Plasticity at Mouse Glutamatergic Synapses

Running title: Mechanisms of Synaptic Zinc Plasticity

Authors: Nathan W. Vogler[1] and Thanos Tzounopoulos[*1]

[1]Pittsburgh Hearing Research Center and Department of Otolaryngology, University of Pittsburgh, Pittsburgh, PA 15261

*Correspondence: thanos@pitt.edu

Keywords: zinc; auditory synapses; synaptic plasticity

Table of Contents category: Neuroscience

Length: 45 pages, plus 7 figures

Funding and Acknowledgements. This work was supported by NIH grants F31-DC015924 (to N.W.V.) and R01-DC007905 (to T.T.). We thank Drs. Stephen Lippard and Jacob Goldberg from Massachusetts Institute of Technology for generously providing DA-ZP1. We thank Patrick Cody and Dr. Ross Williamson for technical help with data analysis. We thank Dr. Elias Aizenman for helpful discussions. The authors declare no competing financial interests.

Key points summary:

- Synaptic zinc is coreleased with glutamate to modulate neurotransmission and auditory processing. Sensory experience causes long-term changes in synaptic zinc signaling, termed synaptic zinc plasticity.
- At zinc-containing glutamatergic synapses in the dorsal cochlear nucleus (DCN), we show that high-frequency stimulation reduces synaptic zinc signaling (Z-LTD), whereas low-frequency stimulation increases synaptic zinc signaling (Z-LTP).
- Group 1 metabotropic glutamate receptor (mGluR) activation is necessary and sufficient to induce Z-LTP and Z-LTD. Z-LTP and Z-LTD are associated with bidirectional changes in presynaptic zinc levels.
- Sound-induced Z-LTD at DCN synapses requires Group 1 mGluR activation.
- Bidirectional synaptic zinc plasticity is a previously unknown mechanism of LTP and LTD at zinc-containing glutamatergic synapses.

Abstract

Synaptic zinc is coreleased with glutamate to modulate neurotransmission in many excitatory synapses. In the auditory cortex, synaptic zinc modulates sound frequency tuning and enhances frequency discrimination acuity. In auditory, visual, and somatosensory circuits, sensory experience causes long-term changes in synaptic zinc levels and/or signaling, termed here *synaptic zinc plasticity*. However, the mechanisms underlying synaptic zinc plasticity and the effects of this plasticity on long-term glutamatergic plasticity remain unknown. To study these mechanisms, we used male and female mice and employed *in vitro* and *in vivo* models in zinc-rich, glutamatergic dorsal cochlear nucleus (DCN) parallel fiber (PF) synapses. High-frequency stimulation of DCN PF synapses induced long-term depression of synaptic zinc signaling (Z-LTD), as evidenced by reduced zinc-mediated inhibition of AMPA receptor (AMPAR) excitatory postsynaptic currents (EPSCs). Low-frequency stimulation induced long-term potentiation of synaptic zinc signaling (Z-LTP), as evidenced by enhanced zinc-mediated inhibition of AMPAR EPSCs. Thus, Z-LTD is a new mechanism of LTP and Z-LTD is a new mechanism of LTP. Pharmacological inhibition of Group 1 metabotropic glutamate receptors (G1 mGluRs) eliminated Z-LTD and Z-LTP. Pharmacological activation of G1 mGluRs induced Z-LTD and Z-LTP, associated with bidirectional changes in presynaptic zinc levels. Finally, exposure of mice to loud sound caused G1 mGluR-dependent Z-LTD in DCN PF synapses, consistent with our *in vitro* results. Together, we show that G1 mGluR activation is necessary and sufficient for inducing bidirectional long-term synaptic zinc plasticity.

Introduction

In many brain areas, including the neocortex, limbic structures, and the auditory brainstem, glutamatergic vesicles are loaded with zinc (Danscher & Stoltenberg, 2005; Frederickson *et al.*, 2005). This pool of mobile, synaptic zinc is coreleased with glutamate. Synaptically released zinc inhibits synaptic and extrasynaptic NMDA receptor (NMDAR) EPSCs, and modulates AMPA receptor (AMPAR) EPSCs (Vogt *et al.*, 2000; Vergnano *et al.*, 2014; Anderson *et al.*, 2015; Kalappa *et al.*, 2015; Kalappa & Tzounopoulos, 2017). Namely, synaptic zinc inhibits AMPAR EPSCs during baseline synaptic activity via postsynaptic mechanisms, but enhances steady-state AMPAR EPSCs during higher frequencies of synaptic stimulation (Kalappa *et al.*, 2015; Kalappa & Tzounopoulos, 2017). The enhancing effect of synaptic zinc on AMPAR EPSCs is short-lasting and is mediated by short-term, zinc-mediated changes in presynaptic glutamatergic neurotransmission (Perez-Rosello *et al.*, 2013; Kalappa & Tzounopoulos, 2017). Thus, synaptic zinc is a major modulator of baseline neurotransmission and short-term plasticity of glutamatergic synapses.

In awake mice, synaptic zinc enhances the responsiveness (gain) of auditory cortical principal neurons to sound, but reduces the gain of cortical interneurons (Anderson *et al.*, 2017). Furthermore, synaptic zinc sharpens the sound frequency tuning of auditory cortical principal neurons, and enhances frequency discrimination acuity (Kumar *et al.*, 2019). Sensory experience bidirectionally modulates the levels of vesicular zinc and synaptic zinc signaling in several sensory brain areas (Nakashima & Dyck, 2009; Kalappa *et al.*, 2015; Li *et al.*, 2017; McAllister & Dyck, 2017). In the somatosensory cortex, whisker plucking increases zinc levels, whereas whisker stimulation reduces zinc levels (Brown & Dyck, 2002, 2005). In the primary visual cortex, monocular deprivation increases vesicular zinc

levels (Dyck *et al.*, 2003). In the retina, optic nerve damage increases zinc levels, which in turn inhibit optic nerve regeneration and promote cell death (Li *et al.*, 2017). In the dorsal cochlear nucleus (DCN), an auditory brainstem nucleus, exposure to loud sound reduces vesicular zinc levels and synaptic zinc signaling (Kalappa *et al.*, 2015). Yet, the cellular and molecular mechanisms underlying the long-term experience-dependent plasticity of synaptic zinc signaling, termed here *synaptic zinc plasticity*, and the relationship of synaptic zinc plasticity to long-term glutamatergic synaptic plasticity remain unknown. Elucidating these mechanisms is crucial for understanding how the brain adapts during normal sensory processing, and why it fails to properly adjust in sensory disorders associated with pathological central adaptation, such as in tinnitus (Auerbach *et al.*, 2014).

To determine the mechanisms of long-term synaptic zinc plasticity and its effects on LTP and LTD, we developed *in vitro* and *in vivo* models. Namely, we used electrophysiology, pharmacology, and fluorescent imaging in the DCN, which contains granule cell endings, parallel fibers (PFs), with high levels of synaptic zinc (Frederickson *et al.*, 1988; Rubio & Juiz, 1998; Kalappa *et al.*, 2015). We investigated these mechanisms *in vitro*, in response to electrical synaptic activation that induces synaptic plasticity such as LTP and LTD in brain slices, as well as *in vivo*, in response to loud sound exposure. Our results demonstrate that bidirectional activity-dependent synaptic zinc plasticity is a previously unknown, Group 1 mGluR-dependent mechanism of LTP and LTD at zinc-containing glutamatergic synapses.

125 **Materials and Methods**

126 **Animals.** Male or female ICR mice (Envigo) were used in this study, aged between
127 postnatal day 17 (P17) to P28. All animal procedures were approved by the Institutional
128 Animal Care and Use Committee of the University of Pittsburgh, Pittsburgh, PA.

129

130 **Brain slice preparation.** Mice were deeply anesthetized with isoflurane (3% in O_2), then
131 immediately decapitated and their brains were removed. Brain slices were prepared in
132 artificial cerebrospinal fluid (ACSF, 34°C) containing the following (in mM): 130 NaCl, 3
133 KCl, 1.2 $CaCl_2 \cdot 2H_2O$, 1.3 $MgCl_2 \cdot 6H_2O$, 20 $NaHCO_3$, 3 HEPES, and 10 D-Glucose,
134 saturated with 95% O_2/5% CO_2 (vol/vol), pH = 7.25-7.35, ~300 mOsm. Using a Vibratome
135 (VT1200S; Leica), coronal brain slices (210 μm thickness) containing the left dorsal
136 cochlear nucleus (DCN) were cut, then placed in a chamber containing warm (34°C)
137 ACSF, and incubated for 60 min at 34°C, then room temperature (no longer than 3 hours)
138 before beginning electrophysiology experiments. Incubating ACSF was the same as
139 cutting ACSF, except it was stirred with Chelex 100 resin (Bio-Rad) for 1 hour to remove
140 contaminating zinc, then filtered using Nalgene rapid flow filters lined with polyethersulfone
141 (0.2 μm pore size). After filtering, high purity $CaCl_2 \cdot 2H_2O$ and $MgCl_2 \cdot 6H_2O$ (99.995%;
142 Sigma Aldrich) were added. All plastic and glassware used for these experiments were
143 washed with 5% nitric acid.

144

145 **Electrophysiology.** *Whole-cell recordings*. DCN slices were transferred to the recording
146 chamber and perfused with ACSF (1-2 mL/min), maintained at ~34°C using an inline
147 heating system (Warner Instruments). Recording ACSF was the same as incubating ACSF
148 (see above), except it contained 2.4 mM $CaCl_2 \cdot 2H_2O$. Whole-cell recordings from
149 cartwheel cells were performed using glass micropipettes (3-6 MΩ; Sutter Instruments).

150 Cartwheel cells were identified by the presence of complex spikes in cell-attached
151 configuration before break-in or in response to current injections in current-clamp mode
152 after break-in (Zhang & Oertel, 1993; Manis *et al.*, 1994; Tzounopoulos *et al.*, 2004).
153 Recording pipettes were filled with a potassium-based internal solution (except for Figure
154 6, see below) containing the following (in mM): 113 K-gluconate, 4.5 $MgCl_2 \cdot 6H_2O$, 14 Tris-
155 phosphocreatine, 9 HEPES, 0.1 EGTA, 4 Na_2ATP, 0.3 Tris-GTP, and 10 sucrose (pH =
156 7.25, 295 mOsm). For experiments shown in Figure 6 measuring NMDAR EPSCs,
157 recordings were performed using a cesium-based internal solution containing the following
158 (in mM): 128 $Cs(CH_3O_3S)$, 10 HEPES, 4 $MgCl_2 \cdot 6H_2O$, 4 Na_2ATP, 0.3 Tris-GTP, 10 Tris-
159 phosphocreatine, 1 EGTA, 1 QX-314, and 3 Na-ascorbate (pH = 7.25, 300 mOsm).
160 Voltages were not corrected for junction potentials. Recordings were performed using
161 ephus (Suter *et al.*, 2010) and a MultiClamp 700B amplifier (Axon Instruments). Data were
162 sampled at 10 kHz and low-pass-filtered at 4 kHz. Series resistance (R_s) and input
163 resistance (R_m) were monitored during the recording period by delivering -5 mV voltage
164 steps for 50 ms. R_s was calculated by dividing the -5 mV voltage step by the peak current
165 generated immediately after the voltage step. R_m was calculated by dividing the -5 mV
166 voltage step by the difference between the baseline and steady-state hyperpolarized
167 current, then subtracting R_s. Data were excluded if R_s or R_m changed by more than 20%
168 from the baseline period. EPSCs were evoked using an Isoflex stimulator (A.M.P.I., 0.1 ms
169 pulses) through a glass ACSF-containing theta electrode to stimulate the zinc-rich parallel
170 fibers. All EPSCs were recorded in the presence of SR95531 (20 μM, $GABA_AR$ antagonist)
171 and strychnine (1 μM, GlyR antagonist). AMPAR EPSCs were recorded in voltage-clamp
172 mode at -70 mV. For paired-pulse experiments, the inter-stimulus interval was 50 ms.
173 NMDAR EPSCs were evoked by a 5-pulse stimulus train (20 Hz) (Anderson *et al.*, 2015),

174 recorded in voltage clamp mode at +40 mV, and in the presence of DNQX (20 μM,
175 AMPA/kainate receptor antagonist). All drugs were always bath applied.

176 *Induction of plasticity*. High-frequency stimulation (HFS) consisted of 3 trains of 100
177 Hz pulses for 1 sec, with 10 sec between trains. For the experiments shown in Figure 1 C,
178 a subset of cells (n=5) were depolarized to -10 mV during each HFS train, while the other
179 subset (n=6) were held at -70 mV during HFS. Because we observed no difference in the
180 zinc plasticity (% potentiation by ZX1) between these subsets (depolarized = 2.68 ±
181 5.36%, non-depolarized = 8.76 ± 8.64%, p = 0.58, unpaired t test), they were grouped
182 together for subsequent analysis. ZX1 (100 μM) is a fast, high-affinity extracellular zinc
183 chelator (Anderson *et al.*, 2015; Kalappa *et al.*, 2015; Kalappa & Tzounopoulos, 2017). For
184 all other experiments, cells were voltage-clamped at -70 mV during HFS. For experiments
185 measuring NMDAR EPSCs after HFS (Figure 6), DNQX (20 μM) was added after HFS,
186 then cells were voltage-clamped at +40 mV to record NMDAR EPSCs. For ifenprodil
187 experiments (Figure 6 D-E), ZX1 was applied prior to ifenprodil to chelate extracellular
188 zinc, because zinc affects NMDAR ifenprodil sensitivity (Hansen *et al.*, 2014). In these
189 experiments after HFS, ZX1 was applied with DNQX, after the HFS. Low-frequency
190 stimulation (LFS) consisted of 5 Hz pulses for 3 min. During LFS, cells were held at -80
191 mV in current-clamp mode. To isolate mGluR-mediated plasticity, all LFS experiments
192 were performed in the presence of APV (50 μM, NMDAR antagonist), and with external
193 ACSF containing 4 mM $CaCl_2 \cdot 2H_2O$ and 4 mM $MgCl_2 \cdot 6H_2O$ (Oliet *et al.*, 1997). The
194 interleaved experiments shown in Figure 4 D, examining the effect of 50 μM DHPG
195 application, were also performed in these conditions. For normalized EPSCs (% baseline),
196 EPSC amplitudes were normalized to the average EPSC amplitude during the 5 min
197 baseline period before HFS/LFS, DHPG, ifenprodil, or ZX1 application. To quantify ZX1

198 potentiation after HFS/LFS or DHPG application, EPSC amplitudes were renormalized to
199 the average EPSC amplitude of the new baseline period 5 min before ZX1 application.
200 ZX1 potentiation (shown in bar graphs) was quantified as the percent increase in the
201 average EPSC amplitude during the last 5 min of ZX1 application compared to the 5 min
202 baseline period before ZX1 application.
203
204 **Vesicular zinc imaging with DA-ZP1.** After preparation and incubation of DCN slices
205 (described above), slices were transferred to the imaging chamber and perfused with
206 recirculating ACSF (2-3 mL/min) maintained at ~34°C. Imaging of presynaptic vesicular
207 zinc levels in DCN parallel fibers was performed using DA-ZP1, a high-affinity, membrane
208 permeable fluorescent zinc sensor (Zastrow *et al.*, 2016). DA-ZP1 (0.5-1.0 μM) was added
209 to the ACSF, and allowed to incubate for at least 20 min before imaging. Images were
210 acquired using an upright microscope (Olympus BX5) with epifluorescence optics through
211 a 20x water immersion objective (Olympus). Green fluorescent signals were isolated using
212 a Pinkel filter set (Semrock LF488/543/625-3X-A-000) in response to excitation by an
213 ephus-driven blue LED (M470L2; Thorlabs), and images were acquired using a CCD
214 camera (Retiga 2000R, QImaging). Images consisted of 20 frames captured at 0.067 Hz
215 which were then averaged together and analyzed in MATLAB (Mathworks). The DCN
216 molecular layer, which contains the vesicular zinc-rich parallel fibers, extends ~75 μm
217 deep from the ependymal surface, while deeper layers lack vesicular zinc (zinc-free
218 region) (Ryugo & Willard, 1985; Frederickson *et al.*, 1988; Rubio & Juiz, 1998). Thus, DA-
219 ZP1 produces a band of fluorescence within the molecular layer near the ependymal
220 surface, consistent with the distribution of zinc-rich parallel fiber terminals (Frederickson *et*
221 *al.*, 1988; Kalappa *et al.*, 2015; Zastrow *et al.*, 2016). The DA-ZP1 fluorescence band is
222 absent in ZnT3 KO mice lacking vesicular zinc, indicating that it specifically labels vesicular

223 zinc (Kalappa *et al.*, 2015; Zastrow *et al.*, 2016). To control for slice-to-slice variability in
224 the molecular layer volume, which in turn might lead to variability in DA-ZP1 brightness, we
225 compared DA-ZP1 fluorescence in the same region of the same slice before and after
226 DHPG application (Figure 5). DA-ZP1 fluorescence 15-20 min after DHPG application was
227 normalized to baseline fluorescence before DHPG application. To quantify DA-ZP1
228 fluorescence, we quantified two ROIs within each slice: one within the zinc-containing
229 molecular layer (zinc ROI) and the other within the zinc-free region (zinc-free ROI)
230 (Kalappa *et al.*, 2015; Zastrow *et al.*, 2016). Because the DCN molecular layer is curved
231 along the ependymal surface, to define the zinc ROI, we used a MATLAB routine to
232 automatically detect the abrupt increase in fluorescence intensity between the background
233 and the ependymal surface of the slice. Then the zinc ROI was automatically selected to
234 include 50 μm depth from the ependymal surface, consistent with the extent of the zinc-
235 containing parallel fiber terminals (Frederickson *et al.*, 1988). The length of the ROI was
236 450 μm. The zinc-free ROI was identical to the zinc ROI, except located 200-250 μm from
237 the border of the slice, within the zinc-free region (deep or fusiform cell layers) (Ryugo &
238 Willard, 1985; Frederickson *et al.*, 1988). Thus, all ROIs contained the same cross-
239 sectional area. The automatically generated ROI borders are shown with yellow lines in
240 Figure 5. Fluorescence intensity was averaged within each ROI, and the zinc-sensitive
241 fluorescence was calculated by subtracting the zinc-free ROI fluorescence from the zinc
242 ROI fluorescence.
243
244 **Noise exposure.** Noise exposure was performed based on previously published methods
245 (Kalappa *et al.*, 2015). Sham- or noise-exposed mice were anesthetized using 3%
246 isoflurane during induction and 1-1.5% during maintenance. Noise-exposed mice were
247 exposed for 4 hours to narrow bandpass noise at 116 dB sound pressure level (SPL),

248 centered at 16 kHz with a 1.6 kHz bandwidth. Noise was presented unilaterally (left ear)
249 through a pipette tip inserted into the left ear canal, with the other end attached to a
250 calibrated speaker (CF-1; Tucker Davis Technologies). Insertion of the pipette tip into the
251 ear canal did not produce a seal. Sham-exposed mice underwent an identical procedure
252 except without any noise exposure. For mice given intraperitoneal injections of AIDA (2
253 mg/kg), one injection was given 30 min prior to exposure, and a second injection was
254 given 2 hours later. After noise- or sham-exposure, ABRs were collected and mice
255 recovered from anesthesia, then DCN slices were prepared (within 30 min after exposure).
256
257 **ABRs.** Auditory Brainstem Responses (ABRs) were measured based on previously
258 published methods (Kalappa *et al.*, 2015). ABRs were recorded immediately after noise- or
259 sham-exposure. During ABR measurements, mice were anesthetized using 3% isoflurane
260 during induction and 1-1.5% during maintenance. Mice were placed in a sound attenuating
261 chamber and temperature was maintained at ~37°C using a heating pad. A subdermal
262 electrode was placed at the vertex, the ground electrode placed ventral to the right pinna,
263 and the reference electrode placed ventral to the left pinna (sham- or noise-exposed ear).
264 In noise-exposed mice, because no ABRs were detected when recording from the
265 exposed (ipsilateral) ear, we recorded ABRs from the non-exposed (contralateral) ear
266 (Figure 7 D). For ABR measurements from contralateral ears of noise-exposed mice, the
267 reference electrode was placed ventral to the right pinna (contralateral ear) and the ground
268 electrode placed ventral to the left pinna. ABRs were detected in response to 1 ms click
269 sound stimuli, presented through a pipette tip inserted into the ear canal, with the other
270 end attached to the speaker (CF-1; Tucker Davis Technologies). ABRs were recorded in
271 response to clicks presented in 10 dB steps, ranging from 0-80 dB SPL. 1 ms clicks were
272 presented at a rate of 18.56/sec using System 3 software package from Tucker Davis

273 Technologies, and ABRs were averaged 512 times and filtered using a 300-3,000 Hz
274 bandpass filter. ABR threshold was defined as the lowest stimulus intensity which
275 generated a reliable Wave 1 in the response waveform. Wave 1 amplitude was measured
276 as the peak-to-trough amplitude of the first wave in the ABR waveform (latency ~2 ms), in
277 response to 80 dB SPL clicks.
278
279 **Drugs.** All chemicals used for ACSF and internal solutions were purchased from Sigma-
280 Aldrich. The following drugs were purchased from HelloBio: SR95531 hydrobromide, DL-
281 AP5, DNQX disodium salt, ifenprodil, MPEP hydrochloride, LY367385, and (S)-3,5-
282 Dihydroxyphenylglycine (DHPG). Strychnine hydrochloride was purchased from Abcam.
283 (RS)-1-Aminoindan-1,5-dicarboxylic acid (AIDA) was purchased from Tocris. ZX1 was
284 purchased from STREM Chemicals.
285
286 **Statistical Analysis**
287 All data analysis was performed using Matlab (Mathworks), Excel (Microsoft), or Prism 7
288 (GraphPad). For statistical tests for normalized data, or within groups, we used one-
289 sample *t* tests (for normally distributed data) or Wilcoxon signed rank tests (for non-
290 normally distributed data). Data were considered normally distributed if they passed the
291 Shapiro-Wilk normality test. For comparisons between two (normally distributed) groups,
292 we used unpaired *t* tests. All *t* tests were two-tailed. For comparisons between three
293 groups, we used ordinary one-way ANOVA with Bonferroni's multiple comparisons test (for
294 normally distributed data), or Kruskal-Wallis test with Dunn's multiple comparisons test (for
295 non-normally distributed data). IC_{50} was calculated using the Hill equation by fitting the
296 dose-response curve with a nonlinear least squares fit. The IC_{50} of each fit was compared

297 using the extra sum-of-squares F test. Significance levels are defined as $p < 0.05$. Group
298 data are presented as mean ± SEM.
299
300 *Detailed values and statistical tests for Figures*. Figure 1: **(1C)** EPSC % baseline after HFS
301 (average of mins. 19-23): 115.1 ± 6.43%, n=11, t=2.34 df=10, *p=0.041, one-sample t test
302 vs. 100%. **(1D)** ZX1 potentiation (%): 'Control': 34.47 ± 5.7%, n=10, t=6.049 df=9,
303 *p=0.0002, one-sample t test vs. 0%. 'HFS': 6.0 ± 5.15%, n=11, t=1.165 df=10, n.s.
304 p=0.27, one-sample t test vs. 0%. 'Control' vs. 'HFS': t=3.719 df=19, *p=0.0015, unpaired t
305 test.
306 Figure 2: **(2A)** EPSC % baseline after HFS (average of mins. 19-23): 124.8 ± 4.76%, n=9,
307 t=5.198 df=8, *p=0.0008, one-sample t test vs. 100%. **(2B)** EPSC % baseline after HFS
308 (average of mins. 19-23): 126.2 ± 9.54%, n=6, t=2.743 df=5, *p=0.041, one-sample t test
309 vs. 100%. One cell was included for analysis of EPSCs following HFS, but did not remain
310 stable throughout subsequent ZX1 application and was excluded from analysis following
311 ZX1 application, quantified in C. **(2C)** ZX1 potentiation (%): 'HFS + APV': 4.28 ± 6.08%,
312 n=9, t=0.7039 df=8, n.s. p=0.502, one-sample t test vs. 0%. 'HFS + LY367385, MPEP,
313 APV': 36.07 ± 9.05%, n=5, t=3.987 df=4, *p=0.016, one-sample t test vs. 0%. One-way
314 ANOVA: F= 7.737, *p=0.003. 'Control' vs. 'HFS + APV': *p=0.0038; 'HFS + APV' vs. 'HFS
315 + LY367385, MPEP, APV': *p= 0.0115; Bonferroni's multiple comparisons test.
316 Figure 3: **(3A)** EPSC % baseline after LFS (average of mins. 19-23): 95.97 ± 3.5%, n=8,
317 t=1.155 df=7, n.s. p=0.29, one-sample t test vs. 100%. Two cells were included for
318 analysis of EPSCs following LFS, but did not remain stable throughout subsequent ZX1
319 application and were excluded from analysis following ZX1 application, quantified in C.
320 **(3B)** EPSC % baseline after LFS (average of mins. 20-24): 73.67 ± 5.8%, n=6, t=4.528
321 df=5, *p=0.006, one-sample t test vs. 100%. **(3C)** ZX1 potentiation (%): 'Control': 19.65 ±

322 4.3%, n=5, t=4.567 df=4, *p=0.01, one-sample t test vs. 0%. 'LFS': 57.86 ± 12.4%, n=6,
323 t=4.681 df=5, *p=0.005, one-sample t test vs. 0%. 'LFS + LY367385, MPEP': 22.18 ±
324 8.3%, n=6, t=2.663 df=5, *p=0.04, one-sample t test vs. 0%. One-way ANOVA: F=5.257,
325 *p=0.0198. 'Control' vs. 'LFS': *p=0.0276; 'LFS' vs. 'LFS + LY367385, MPEP': *p=0.0309;
326 Bonferroni's multiple comparisons test.
327 Figure 4: **(4A)** EPSC % baseline after 50 μM DHPG (average of mins. 16-20): 49.66 ±
328 5.1%, n=6, t=9.945 df=5, *p=0.0002, one-sample t test vs. 100%. One cell was included for
329 analysis of EPSCs following 50 μM DHPG, but did not remain stable throughout
330 subsequent ZX1 application and was excluded from analysis following ZX1 application,
331 quantified in C. **(4B)** EPSC % baseline after 5 μM DHPG (average of mins. 16-20): 82.41 ±
332 7.4%, n=5, t=2.376 df=4, n.s. p=0.076, one-sample t test vs. 100%. **(4C)** ZX1 potentiation
333 (%): 'DHPG (50 μM)': 93.51 ± 10.92%, n=5, t=8.561 df=4, *p=0.001, one-sample t test vs.
334 0%. 'DHPG (5 μM)': 0.44 ± 7.08%, n=5, t=0.06273 df=4, n.s. p=0.95, one-sample t test vs.
335 0%. One-way ANOVA: F=30.22, *p<0.0001. 'Control' vs. 'DHPG (50 μM)': *p<0.0001;
336 'Control' vs. 'DHPG (5 μM)': *p=0.01; Bonferroni's multiple comparisons test. **(4D)** EPSC %
337 baseline after 50 μM DHPG (average of mins. 16-20): 83.05 ± 5.9%, n=5, t=2.893 df=4,
338 *p=0.044, one-sample t test vs. 100%. **(4E)** EPSC % baseline after LFS and 50 μM DHPG
339 (average of mins. 20-24): 81.43 ± 9.1%, n=5, t=2.051 df=4, n.s. p=0.11, one-sample t test
340 vs. 100%. **(4F)** ZX1 potentiation (%): 'DHPG (50 μM)': 55.83 ± 17.9%, n=5, t=3.12 df=4,
341 *p=0.036, one-sample t test vs. 0%. 'LFS + DHPG (50 μM)': 74.65 ± 17.6%, n=5, t=4.246
342 df=4, *p=0.013, one-sample t test vs. 0%. One-way ANOVA: F=0.4126, n.s. p=0.6703.
343 'LFS + DHPG (50 μM)' vs. 'LFS': n.s. p=0.9181; 'LFS + DHPG (50 μM)' vs. 'DHPG (50
344 μM)': n.s. p=0.8553; Bonferroni's multiple comparisons test.

345 Figure 5: **(5C)** DA-ZP1 fluorescence (% control): '+ DHPG (50 μM)': 132.3 ± 9.096%, n=9,
346 *p=0.0039, Wilcoxon signed rank test vs. 100%. '+ DHPG (5 μM)': 68.73 ± 11.99%, n=8,
347 *p=0.0078, Wilcoxon signed rank test vs. 100%.
348 Figure 6: **(6C)** ZX1 potentiation (%): 'Control': 37.1 ± 3.1%, n=5, t=12.06 df=4, *p=0.0003,
349 one-sample t test vs. 0%. 'HFS': 9.2 ± 5.2%, n=6, n.s. p=0.16, Wilcoxon signed rank test
350 vs. 0%. 'HFS + LY267385, MPEP': 42.6 ± 8.2%, n=5, t=5.197 df=4, *p=0.007, one-sample
351 t test vs. 0%. Kruskal-Wallis test: *p=0.0102. 'Control' vs. 'HFS': *p=0.0242; 'HFS' vs. 'HFS
352 + LY367385, MPEP': *p=0.0428; Dunn's multiple comparisons test. **(6D)** EPSC (%
353 baseline): 'Control': 300nM: n=3, 90.68 ± 1.051%; 1μM: n=5, 70.89 ± 3.943%; 3μM: n=5,
354 54.61 ± 2.791%; 10μM: n=3, 40.72 ± 4.845%. 'HFS': 300nM: n=3, 90.24 ± 4.327%; 1μM:
355 n=4, 69.52 ± 2.208%; 3μM: n=4, 52.1 ± 3.214%; 10μM: n=3, 37.89 ± 1.533%. Nonlinear
356 fits: 'Control': Hill Slope=1.095, R^2=0.9472. 'HFS': Hill Slope=1.128, R^2=0.9765. **(6E)** IC_{50}
357 (μM): 'Control': 1.284 ± 0.3566. 'HFS': 1.267 ± 0.2321. Extra sum-of-squares F test: n.s.
358 p=0.9687.
359 Figure 7: **(7B)** ZX1 potentiation (%): 'N.E.': 11.7 ± 8.56%, n=5, t=1.373 df=4, n.s. p=0.24,
360 one-sample t test vs. 0%. 'N.E. + AIDA': 43.8 ± 8.05%, n=6, t=5.447 df=5, *p=0.003, one-
361 sample t test vs. 0%. 'N.E.' vs. 'N.E. + AIDA': t=2.724 df=9, *p=0.024, unpaired t test. **(7C)**
362 PPR: 'N.E.': 1.896 ± 0.19, n=5. 'N.E. + AIDA: 2.056 ± 0.12, n=6. 'N.E.' vs. 'N.E. + AIDA':
363 t=0.7446 df=9, n.s. p=0.476, unpaired t test. Normalized $1/CV^2$: 'N.E. + AIDA': 0.78 ± 0.22,
364 n=6; n.s. p=0.44, Wilcoxon signed rank test vs. 1. **(7E)** ABR threshold (dB SPL): 'Sham
365 ipsi.': 43.75 ± 3.24, n=8. 'N.E. contra.': 68.33 ± 3.07, n=6. 'N.E. + AIDA contra.': 65.71 ±
366 2.97, n=7. Kruskal-Wallis test: *p=0.0002. 'Sham ipsi.' vs. 'N.E. contra.': *p=0.0042; 'Sham
367 ipsi.' vs. 'N.E. + AIDA contra.': *p=0.0076; 'N.E. contra.' vs. 'N.E. + AIDA contra.': n.s.
368 p>0.9999; Dunn's multiple comparisons test. ABR Wave I (μV): 'Sham ipsi.': 2.67 ± 0.31,

369 n=8. ‘N.E. contra.’: 1.23 ± 0.13, n=6. ‘N.E. + AIDA contra.’: 1.25 ± 0.27, n=7. Kruskal-
370 Wallis test: *p=0.0024. ‘Sham ipsi.’ vs. ‘N.E. contra.’: *p= 0.0387; ‘Sham ipsi.’ vs. ‘N.E. +
371 AIDA contra.’: *p=0.0107; ‘N.E. contra.’ vs. ‘N.E. + AIDA contra.’: n.s. p>0.9999; Dunn's
372 multiple comparisons test.
373
374 **Results**
375 **Bidirectional activity-dependent long-term synaptic zinc plasticity requires Group 1**
376 **mGluR activation.** To investigate the mechanisms underlying synaptic zinc plasticity, we
377 first determined whether we could induce long-term synaptic zinc plasticity in DCN PF
378 synapses in mouse brain slices. In these synapses, synaptic zinc inhibits AMPAR and
379 NMDAR EPSCs via postsynaptic mechanisms. This has been evidenced by application of
380 ZX1, a fast, high-affinity extracellular zinc chelator, which potentiates AMPAR and NMDAR
381 EPSCs (Anderson *et al.*, 2015; Kalappa *et al.*, 2015; Kalappa & Tzounopoulos, 2017). This
382 *ZX1 potentiation* of AMPA and NMDAR EPSCs is dependent on ZnT3, the transporter that
383 loads zinc into synaptic vesicles (Palmiter *et al.*, 1996; Cole *et al.*, 1999). Moreover,
384 reductions in ZX1 potentiation reflect reductions in synaptic zinc levels and release
385 (Kalappa *et al.*, 2015). Therefore, in this study, we used the amount of ZX1 potentiation of
386 AMPAR and NMDAR EPSCs to monitor synaptic zinc signaling, and long-term synaptic
387 zinc plasticity, in DCN PF synapses.
388
389 Consistent with previous studies, we found that ZX1 potentiated postsynaptic PF AMPAR
390 EPSCs in DCN cartwheel cells (CWCs), a class of inhibitory interneurons (Figure 1 A-B)
391 (Kalappa *et al.*, 2015; Kalappa & Tzounopoulos, 2017). We then tested whether we can
392 induce long-term synaptic zinc plasticity by using patterns of synaptic activation that induce
393 long-term plasticity of glutamatergic synaptic strength in DCN PF synapses, such as LTP

394 and LTD (Fujino & Oertel, 2003; Tzounopoulos *et al.*, 2004; Tzounopoulos *et al.*,
395 2007). We started by examining the effect of ZX1 on AMPAR EPSCs following high-
396 frequency stimulation of PFs (HFS, 3 x 100 Hz for 1 sec, 10 sec inter-stimulus interval),
397 which induces LTP (Fujino & Oertel, 2003). After applying HFS and inducing LTP (Figure 1
398 C), we renormalized AMPAR EPSC amplitude to quantify the amount of ZX1 potentiation.
399 (Figure 1 C). After HFS, ZX1 application did not potentiate AMPAR EPSCs (Figure 1 C-D).
400 The loss of ZX1 potentiation indicates a loss of zinc-mediated inhibition of AMPARs,
401 suggesting that HFS caused a long-term reduction in synaptic zinc signaling, termed *Z-*
402 *LTD* (Figure 1 D). Furthermore, these results suggest that Z-LTD, by reducing zinc-
403 mediated inhibition of AMPAR EPSCs and thus enhancing baseline synaptic strength, is a
404 new mechanism of HFS-induced LTP. For a discussion on the impact of synaptic zinc
405 plasticity in the context of other long-term plasticity mechanisms, see *Discussion* section,
406 *Implications of Z-LTP and Z-LTD for LTD and LTP*.
407
408 After establishing that HFS caused Z-LTD, we then studied the underlying mechanisms.
409 NMDARs contribute to the induction of LTP and LTD in the DCN and most central
410 synapses (Malenka & Nicoll, 1993; Fujino & Oertel, 2003; Tzounopoulos *et al.*, 2004;
411 Tzounopoulos *et al.*, 2007). To test the role of NMDARs in the induction of Z-LTD, we
412 blocked NMDARs with APV (NMDAR antagonist, 50 μM; Figure 2 A). As evidenced by the
413 lack of ZX1 potentiation of AMPAR EPSCs after HFS, APV did not affect Z-LTD (Figure 2
414 A, C), indicating that NMDARs are not required for the induction of Z-LTD.
415
416 Parallel fiber synapses in the DCN also exhibit glutamatergic plasticity that involves
417 metabotropic glutamate receptor (mGluR) signaling (Fujino & Oertel, 2003). Furthermore,

418 Group 1 (G1) mGluRs are expressed in CWCs and in the DCN molecular layer, where PF
419 terminals reside (Wright *et al.*, 1996; Bilak & Morest, 1998). We therefore tested whether
420 G1 mGluR activation is necessary for Z-LTD. To test this hypothesis, we repeated the
421 experiment shown in Figure 2A, but we now blocked G1 mGluRs with MPEP (4 μM,
422 mGluR5-selective antagonist) and LY367385 (100 μM, mGluR1-selective antagonist)
423 (Figure 2 B). Under these conditions, ZX1 potentiation was observed after HFS, indicating
424 that HFS did not induce Z-LTD (Figure 2 B-C). This result demonstrates that G1 mGluR
425 activation is necessary for the induction of Z-LTD.
426
427 Glutamatergic plasticity is bidirectional: synapses undergo LTP or LTD in response to high-
428 or low-frequency stimulation, respectively (Mulkey & Malenka, 1992; Malenka & Nicoll,
429 1993; Fujino & Oertel, 2003). To determine whether long-term synaptic zinc plasticity is
430 bidirectional, we tested whether low-frequency stimulation (LFS) increases zinc signaling
431 (Figure 3 A). Because the induction of zinc plasticity depends on mGluR activation, we
432 used conditions that favor mGluR-dependent LTD, such as LFS (5 Hz, 3 min), blockade of
433 NMDARs with APV, and high extracellular concentrations of divalent ions (4 mM Ca^{2+} and
434 Mg^{2+}) (Oliet *et al.*, 1997). Compared to interleaved control experiments, LFS increased the
435 amount of subsequent ZX1 potentiation (Figure 3 A, C). Increased ZX1 potentiation
436 indicates increased zinc-mediated inhibition of AMPARs, suggesting that LFS caused a
437 long-term increase in synaptic zinc signaling, termed *Z-LTP* (Figure 3 C). By enhancing
438 zinc-mediated inhibition of AMPAR EPSCs, Z-LTP is a new mechanism of LFS-induced
439 LTD.
440

441 Note that control ZX1 potentiation in these conditions (Figure 3 A, C) was slightly less,
442 albeit not significantly different (p=0.11, unpaired t test), than previous control experiments
443 performed in ACSF with 2.4/1.3 mM of extracellular Ca^{2+}/Mg^{2+} (Figure 1 D). This is likely
444 due to reduced neuronal excitability in higher divalent concentrations (Oliet *et al.*, 1997;
445 Kalappa *et al.*, 2015). Together, these results show that LFS induced Z-LTP, thus
446 demonstrating that activity-dependent plasticity of zinc signaling is bidirectional: HFS
447 induces long-term depression of zinc signaling (Z-LTD), whereas LFS induces long-term
448 potentiation of zinc signaling (Z-LTP).
449
450 We next tested whether G1 mGluR activation is necessary for the induction of Z-LTP. In
451 the presence of MPEP and LY367385, LFS did not increase the amount of ZX1
452 potentiation (Figure 3 B-C), indicating that G1 mGluR activation is necessary for the
453 induction of Z-LTP. Together, these results reveal that activation of G1 mGluR signaling is
454 necessary for the induction of Z-LTP and Z-LTD.
455
456 **Group 1 mGluR activation is sufficient to induce bidirectional long-term synaptic**
457 **zinc plasticity.** Is activation of G1 mGluRs sufficient to induce Z-LTP and Z-LTD?
458 Because G1 mGluRs are required for both increases and decreases in synaptic zinc
459 signaling by different stimulation paradigms, we hypothesized that the direction of plasticity
460 depends on the differential activation of G1 mGluRs during HFS and LFS. To test this, we
461 applied high or low concentrations of DHPG (G1 mGluR agonist, 50 μM or 5 μM).
462 Consistent with previous studies, application of 50 μM DHPG caused a significant
463 depression of synaptic strength (Figure 4 A) (Huber *et al.*, 2001; Snyder *et al.*, 2001;
464 Wisniewski & Car, 2002). After applying 50 μM DHPG, obtaining a new stable baseline,

465 and then applying ZX1, we observed that the ZX1 potentiation of EPSCs was significantly
466 increased compared to control experiments (Figure 4 A, C). This result indicates that a
467 high concentration of DHPG increases synaptic zinc signaling: G1 mGluR activation is
468 sufficient to induce Z-LTP.
469
470 Because Z-LTP and Z-LTD induced by LFS and HFS depend on G1 mGluR activation
471 (Figure 2 and 3), we next tested whether application of a lower concentration of DHPG
472 causes Z-LTD. After applying 5 μM DHPG and obtaining a new stable baseline, ZX1 did
473 not potentiate EPSCs, consistent with Z-LTD induction (Figure 4 B-C). Together, these
474 results demonstrate that G1 mGluR activation is sufficient to cause bidirectional zinc
475 plasticity. Furthermore, the direction of zinc plasticity depends on the concentration of
476 DHPG: 50 μM DHPG causes Z-LTP, whereas 5 μM DHPG causes Z-LTD (Figure 4 C).
477 These results are consistent with the notion that bidirectional zinc plasticity depends on
478 differential activation of G1 mGluRs by either LFS/HFS or high/low concentrations of
479 DHPG.
480
481 Electrical synaptic stimulation with LFS/HFS or pharmacological activation of G1 mGluRs
482 with high/low concentrations of DHPG induce bidirectional synaptic zinc plasticity;
483 however, it is unknown whether these two different methods induce mechanistically similar
484 synaptic zinc plasticity. To explore this, we compared the amount of Z-LTP elicited by
485 applying sequential LFS and 50 μM DHPG to the amount of Z-LTP elicited by LFS or 50
486 μM DHPG alone. If electrical and pharmacological manipulations induce Z-LTP by different
487 mechanisms, then LFS and 50 μM DHPG application should yield an additive effect on Z-
488 LTP, and subsequent ZX1 potentiation should be greater than that following LFS alone or

489 application of 50 μM DHPG alone. To test this, we performed interleaved experiments to
490 determine the effect of 50 μM DHPG alone, under the conditions used for LFS-induced Z-
491 LTP as in Figure 3, with experiments involving stimulation with LFS and subsequent DHPG
492 application (Figure 4 D-E). Under these conditions, ZX1 potentiation following application
493 of 50 μM DHPG was similar to ZX1 potentiation following LFS (Figure 4 F). Importantly,
494 ZX1 potentiation after sequential LFS and 50 μM DHPG was not significantly greater than
495 ZX1 potentiation after LFS or DHPG alone (Figure 4 F). Together, these results show that
496 LFS occluded the effect of 50 μM DHPG; thus, LFS and DHPG induce Z-LTP likely via a
497 common mechanistic pathway.
498
499 **Group 1 mGluR activation bidirectionally modulates presynaptic zinc levels.** We
500 used activity-dependent changes in the amount of ZX1 potentiation of AMPAR EPSCs for
501 assessing changes in synaptic zinc signaling (Z-LTP and Z-LTD). However, ZX1
502 potentiation is determined by the postsynaptic zinc-mediated inhibition of AMPAR EPSCs,
503 as well as the amount of presynaptic zinc release (Kalappa *et al.*, 2015). Because previous
504 studies demonstrated sensory experience-dependent, long-term modulation of presynaptic
505 zinc levels (Nakashima & Dyck, 2009; Kalappa *et al.*, 2015), we hypothesized that Z-LTP
506 and Z-LTD are expressed, at least in part, by the modulation of presynaptic zinc levels. To
507 quantify potential changes in presynaptic zinc levels, we used DA-ZP1, a fluorescent
508 intracellular zinc sensor capable of tracking presynaptic zinc levels in PF terminals
509 (Kalappa *et al.*, 2015; Zastrow *et al.*, 2016). DA-ZP1 produces a band of fluorescence
510 within the DCN molecular layer in wild type mice. This fluorescent signal is absent in mice
511 lacking the vesicular ZnT3 transporter, thus demonstrating that the signal is due to ZnT3-
512 dependent, synaptic zinc (Kalappa *et al.*, 2015; Zastrow *et al.*, 2016). To induce Z-LTP and

513 Z-LTD, we applied DHPG, which is mechanistically similar to electrically-induced Z-LTP
514 and Z-LTD (Figure 4 F) and capable of inducing robust synaptic zinc plasticity in many
515 terminals in the slice. To test for changes in presynaptic zinc levels, we imaged DA-ZP1
516 fluorescence in the same region of the same DCN slice before and after DHPG application
517 (50 μM or 5 μM) (Figure 5 A; see *Materials and Methods*). Application of 50 μM DHPG
518 increased DA-ZP1 fluorescence, indicating increased presynaptic zinc levels in PF
519 terminals, which is consistent with Z-LTP (Figure 5 A, C). In contrast, application of 5 μM
520 DHPG reduced DA-ZP1 fluorescence, indicating reduced zinc levels, which is consistent
521 with Z-LTD (Figure 5 B-C).
522
523 Together, these results demonstrate that differential activation of G1 mGluRs, by
524 application of different concentrations of DHPG, causes bidirectional modulation of
525 presynaptic zinc levels. Furthermore, these results are consistent with our
526 electrophysiological experiments: 50 μM DHPG results in Z-LTP by increasing presynaptic
527 zinc levels, whereas 5 μM DHPG results in Z-LTD by reducing presynaptic zinc levels.
528 Although these results do not rule out potential postsynaptic mechanisms of Z-LTP and Z-
529 LTD, they demonstrate that Z-LTP and Z-LTD are associated with modulation of
530 presynaptic zinc levels.
531
532 **G1 mGluR-dependent Z-LTD reduces zinc-mediated inhibition of NMDARs.** Z-LTP
533 and Z-LTD involve modulation of presynaptic zinc signaling (Figure 5). Based on this
534 finding, the induction of long-term synaptic zinc plasticity should also affect postsynaptic
535 NMDAR EPSCs, which are inhibited by zinc via direct high-affinity NMDAR allosteric
536 modulation (Paoletti *et al.*, 1997; Vergnano *et al.*, 2014). To test this prediction, we

537 quantified the ZX1 potentiation of NMDAR EPSCs after inducing Z-LTD with HFS. To
538 monitor NMDAR EPSCs, we used a short train of presynaptic stimulation (5 pulses at 20
539 Hz) to activate extrasynaptic NMDARs, for NMDAR EPSCs recorded in somata of CWCs
540 are mostly mediated by extrasynaptic NMDARs activated by glutamate spillover during this
541 short train (Anderson *et al.*, 2015). To avoid keeping CWCs at +40 mV for too long while
542 recording NMDAR EPSCs, and to maintain the same induction protocol used in our
543 previous experiments, we initially recorded AMPAR EPSCs at -70 mV and then applied
544 HFS (Figure 6 A). Subsequently, we blocked AMPARs with DNQX (20 μM, AMPA/kainate
545 receptor antagonist) and recorded at +40 mV to obtain a stable baseline of NMDAR
546 EPSCs before applying ZX1 (Figure 6 A). Consistent with our results on AMPAR EPSCs,
547 after HFS, ZX1 no longer potentiated NMDAR EPSCs, whereas ZX1 potentiated NMDAR
548 EPSCs in interleaved control experiments, where HFS was not applied (Figure 6 A, C).
549 These results demonstrate that Z-LTD reduces zinc-mediated inhibition of NMDARs. To
550 determine whether this plasticity shares the same mechanism as Z-LTD evidenced by
551 changes in the ZX1 potentiation of AMPAR EPSCs, we tested whether G1 mGluR
552 signaling is required. Indeed, application of MPEP and LY367385 blocked the observed Z-
553 LTD, evidenced by the ZX1 potentiation of NMDAR EPSCs after HFS (Figure 6 B-C).
554 Together, our results suggest that G1 mGluR-dependent synaptic zinc plasticity modulates
555 zinc-mediated inhibition of AMPARs and NMDARs similarly, suggesting that it is
556 independent of the mode of action of synaptic zinc on its postsynaptic targets. This
557 supports our findings that zinc plasticity is expressed, at least in part, by changes in
558 presynaptic zinc levels.
559
560 However, the contribution of postsynaptic mechanisms in synaptic zinc plasticity cannot be
561 excluded. To address this possibility, we tested whether activity-dependent changes in

562 postsynaptic NMDAR subunit composition could modulate zinc sensitivity. NMDARs are
563 composed of two GluN1 subunits and two GluN2 subunits (Traynelis *et al.*, 2010). GluN2A-
564 containing NMDARs (GluN1/GluN2A diheteromers and GluN2/GluN2A/GluN2B
565 triheteromers) have nanomolar affinity for zinc, whereas GluN1/GluN2B diheteromers have
566 micromolar affinity (Paoletti *et al.*, 1997; Rachline *et al.*, 2005; Tovar & Westbrook, 2012;
567 Hansen *et al.*, 2014). Therefore, the reduced zinc-mediated inhibition of NMDAR EPSCs
568 after HFS, evidenced by reduced ZX1 potentiation (Figure 6 A), could be explained by an
569 increase in the proportion of GluN2B subunits. We therefore tested whether HFS increases
570 the sensitivity of NMDAR EPSCs to ifenprodil, a GluN2B-selective antagonist (Figure 6 D-
571 E) (Tovar & Westbrook, 2012; Hansen *et al.*, 2014). Compared to controls, HFS did not
572 affect the ifenprodil sensitivity (IC_{50}) of NMDAR EPSCs (Figure 6 D-E). This indicates that
573 HFS-induced plasticity does not alter the proportions of GluN2B vs. GluN2A NMDAR
574 subunits, suggesting that Z-LTD is not due to reduced zinc sensitivity caused by a
575 decrease in the relative contribution of GluN2A vs. GluN2B in the NMDAR EPSC.
576 Therefore, these results further support that zinc plasticity is expressed by changes in
577 presynaptic zinc levels, rather than postsynaptic receptor modifications.
578
579 **Sound-induced zinc plasticity requires Group 1 mGluRs *in vivo.*** Our experiments
580 described here, using *in vitro* brain slice electrophysiology in the DCN point toward a
581 mechanism of bidirectional long-term synaptic zinc plasticity dependent on G1 mGluR
582 activation. We therefore hypothesized that G1 mGluR activation may also be necessary for
583 the reduction in synaptic zinc signaling observed in the DCN after sound exposure
584 (Kalappa *et al.*, 2015). To test this hypothesis, we quantified the ZX1 potentiation of PF
585 EPSCs in DCN slices from mice exposed to loud sound (116 dB, 4 hours). Consistent with
586 sound-induced LTD and previous studies (Kalappa *et al.*, 2015), we did not observe ZX1

587 potentiation in slices from noise-exposed (N.E.) mice (Figure 7 A-B). To test whether G1
588 mGluRs are necessary for the reduced zinc signaling in slices from N.E. mice, we
589 administered a systemic, blood brain barrier-permeable G1 mGluR antagonist (AIDA, i.p.,
590 2 mg/kg; twice: 30 min before and 1.5 hours after beginning the noise exposure). Indeed,
591 we observed ZX1 potentiation in slices from N.E. mice treated with AIDA (Figure 7 A-B),
592 suggesting that *in vivo* inhibition of G1 mGluR activity blocked the sound-induced Z-LTD.
593
594 Although AIDA treatment blocked Z-LTD in DCN PF synapses (Figure 7 A-B), it did not
595 affect assays that are sensitive to presynaptic glutamate release probability, such as
596 paired-pulse ratio (PPR) and coefficient of variation (CV) analysis (Figure 7 C). This
597 indicates that sound-induced G1 mGluR-dependent Z-LTD specifically modulates synaptic
598 zinc signaling, without affecting presynaptic glutamate signaling in PFs. Furthermore, AIDA
599 treatment did not affect sound-induced hearing loss in N.E. mice, quantified with Auditory
600 Brainstem Responses (ABRs) (Figure 7 D). ABRs reflect the synchronous activity, arising
601 from the auditory nerve (Wave I), of auditory brainstem nuclei to the inferior colliculus
602 (Waves II-V) in response to sound stimuli. Elevated ABR thresholds indicate increased
603 hearing thresholds. However, similar ABR thresholds may be accompanied by differences
604 in the suprathreshold response of Wave I, which could reflect differential degeneration of
605 the auditory nerve (Kujawa & Liberman, 2009). AIDA treatment did not affect noise-
606 induced changes in either ABR thresholds or Wave I amplitude (Figure 7 E), thus
607 indicating that the effect of AIDA on blocking Z-LTD is not due to differential noise-induced
608 hearing loss after AIDA treatment. Together, these results demonstrate that sound-induced
609 Z-LTD requires G1 mGluR activation, consistent with our *in vitro* results.
610
611

612 **Discussion**

613 Our results show that long-term synaptic zinc plasticity is an experience-, G1 mGluR-
614 dependent mechanism that bidirectionally modulates synaptic zinc signaling in the DCN. Is
615 this a general mechanism that applies to all synaptic zinc-containing brain areas? Synaptic
616 zinc is present throughout the neocortex and other brain structures, such as the amygdala
617 and the hippocampus (McAllister & Dyck, 2017). Moreover, synaptic zinc is modulated by
618 sensory activity throughout the sensory cortex (McAllister & Dyck, 2017), shapes the gain
619 of central sensory responses (Anderson *et al.*, 2017), and when upregulated by optic nerve
620 injury, it inhibits retinal ganglion cell survival and axon regeneration (Li *et al.*, 2017). It is
621 therefore likely, although not tested here, that the reported long-term synaptic zinc
622 plasticity mechanism is a general mechanism that dynamically modulates sensory
623 processing for adaptation to different sensory environments and injury.

624

625 Whereas the exact synaptic, natural, and ethologically relevant stimuli that elicit Z-LTP and
626 Z-LTD remain unknown, here we developed *in vitro* and *in vivo* models for studying Z-LTP
627 and Z-LTD. This is a crucial step towards further elucidation of the detailed natural stimuli
628 eliciting long-term synaptic zinc plasticity, as well as the precise cellular and molecular
629 mechanisms underlying the induction and expression of Z-LTP and Z-LTD. Moreover, our
630 model will be useful for probing the unknown behavioral consequences of Z-LTP and Z-
631 LTD.

632

633 **Mechanisms of Group 1 mGluR-dependent Z-LTP and Z-LTD.** Our results show that
634 differential activation of G1 mGluRs, by either LFS/HFS or high/low concentrations of
635 DHPG, determines the induction and direction of long-term synaptic zinc plasticity.
636 Prolonged LFS causes Z-LTP, similarly to G1 mGluR activation with 50 μM DHPG;

637 whereas, brief HFS causes Z-LTD, similarly to activation with 5 μM DHPG. This suggests
638 that prolonged LFS activates G1 mGluR signaling differently than brief HFS.
639
640 Group 1 mGluRs, mGluR1 and mGluR5, are linked to the IP_3-Diacylglycerol (DAG)
641 signaling pathway, leading to intracellular rises in Ca^{2+} from intracellular stores (Abdul-
642 Ghani *et al.*, 1996; Conn & Pin, 1997; Kim *et al.*, 2008). In the hippocampus, LFS induces
643 G1 mGluR-mediated LTD via postsynaptic AMPAR endocytosis involving Ca^{2+} release
644 from endoplasmic reticulum (ER) stores and dendritic protein synthesis (Huber *et al.*, 2000;
645 Holbro *et al.*, 2009; Luscher & Huber, 2010; Pick & Ziff, 2018). Moreover, in the
646 hippocampus, HFS or theta-burst stimulation induces G1 mGluR-mediated LTP, also
647 involving ER Ca^{2+} release, resulting in postsynaptic AMPAR/NMDAR trafficking or
648 enhanced presynaptic glutamate release (Topolnik *et al.*, 2006; Wu *et al.*, 2008; Anwyl,
649 2009). It remains unknown whether G1 mGluR-dependent Z-LTP and Z-LTD are
650 downstream effects of the same signaling pathways that induce LTD and LTP, or occur
651 through separate mechanisms. Nonetheless, we propose, albeit not tested here, that
652 differential G1 mGluR activation, by LFS/HFS, leads to subsequent release of different
653 amounts or types of intracellular Ca^{2+} signals. Different Ca^{2+} signals may in turn activate
654 diverse signaling pathways that ultimately lead to increased and decreased synaptic zinc
655 signaling. An analogue that comes to mind is the mechanism via which differential
656 activation of NMDARs, by various levels of synaptic activity, leads to variable Ca^{2+} levels
657 and signaling, ultimately determining the induction of both LTP and LTD (Malenka & Bear,
658 2004).
659
660 Our results suggest that increases or decreases in synaptic zinc signaling, evidenced by
661 increased or decreased ZX1 potentiation of EPSCs, are mediated by bidirectional

662 modulation of vesicular zinc levels and subsequent synaptic zinc release. High or low
663 concentrations of DHPG, which induce Z-LTP and Z-LTD, increase or decrease
664 presynaptic zinc levels in PF terminals (Figure 5). Furthermore, synaptic zinc plasticity
665 modulates zinc-mediated inhibition of NMDARs as well as AMPARs, and this effect on
666 NMDARs cannot be explained by postsynaptic changes in the relative contributions of
667 GluN2A vs. GluN2B subunits in the NMDAR EPSCs (Figure 6). Although we cannot fully
668 exclude potential contributions of postsynaptic mechanisms in synaptic zinc plasticity, our
669 results support that synaptic zinc plasticity is mainly mediated by activity-dependent
670 modulation of presynaptic zinc levels and signaling, and are consistent with previous
671 studies demonstrating experience-dependent modulation of vesicular zinc levels in the
672 somatosensory cortex (Brown & Dyck, 2002, 2005), visual cortex (Dyck *et al.*, 2003), optic
673 nerve (Li *et al.*, 2017), and the DCN (Kalappa *et al.*, 2015).
674
675 Cartwheel cells express G1 mGluRs, particularly mGluR1, suggesting that the locus of
676 induction of zinc plasticity is postsynaptic (Wright *et al.*, 1996). Because Z-LTP and Z-LTD
677 involve modulation of presynaptic zinc levels, one suggestion is the presence of a
678 retrograde signal from CWCs involved in the expression of Z-LTP and Z-LTD in PFs.
679 Alternatively, the presence of mGluR1 on axon terminals in the DCN molecular layer may
680 support a presynaptic locus of induction (Bilak & Morest, 1998). Because ZnT3 determines
681 vesicular zinc levels (Palmiter *et al.*, 1996; Cole *et al.*, 1999), modulation of ZnT3
682 expression or function may underlie the expression of Z-LTP and Z-LTD. In the retina,
683 optic nerve injury increases ZnT3 immunostaining, supporting that increases in ZnT3
684 expression mediate increases in synaptic zinc levels (Li *et al.*, 2017). However, in the
685 barrel cortex, whisker plucking increases the vesicular zinc content and the density of zinc-
686 containing synapses, but does not alter either ZnT3 protein or mRNA levels (Brown &

687 Dyck, 2002; Liguz-Lecznar *et al.*, 2005; Nakashima & Dyck, 2010; Nakashima *et al.*,
688 2011). Furthermore, in barrel cortical layers IV and V, the density of excitatory synapses
689 remains unchanged despite the increased density of zinc-containing synapses, indicating
690 that some previously excitatory non-zinc-containing synapses were converted to zinc-
691 containing synapses (Nakashima & Dyck, 2010). Together, these studies suggest that
692 changes in vesicular zinc content can occur without affecting glutamatergic synapses,
693 likely via functional modulation of pre-existing ZnT3. This may also explain our
694 electrophysiological results after sound exposure, because sound exposure caused Z-LTD
695 without affecting presynaptic glutamate dynamics (Figure 7 C). In the context of ZnT3
696 modulation, it is interesting that the vesicular glutamate transporter 1 (VGlut1), which is co-
697 targeted to synaptic vesicles with ZnT3, increases ZnT3 zinc transport in cultured cells
698 (Salazar *et al.*, 2005). Because VGlut1 is highly expressed in the DCN molecular layer
699 (Zhou *et al.*, 2007), one hypothesis is that modulation of VGlut1 may modulate ZnT3
700 function in PF terminals. However, the independent modulation of presynaptic glutamate
701 and zinc dynamics after sound exposure (Figure 7 C) suggests a VGlut1-independent
702 mechanism of ZnT3 modulation. While our results reveal a role for G1 mGluRs in Z-LTP
703 and Z-LTD, future experiments will be necessary to determine the detailed induction and
704 expression mechanisms.
705
706 **Implications of Z-LTP and Z-LTD for short-term plasticity.** Previous studies in DCN PF
707 synapses revealed that synaptic zinc triggers endocannabinoid synthesis, which inhibits
708 presynaptic glutamate release and modulates short-term plasticity (Perez-Rosello *et al.*,
709 2013; Kalappa & Tzounopoulos, 2017). During high-frequency (50 Hz) trains, synaptic zinc
710 inhibits AMPAR EPSCs during the first few stimuli, but enhances steady-state EPSCs in
711 subsequent stimuli by recruiting endocannabinoid signaling and enhancing synaptic

712 facilitation (Kalappa & Tzounopoulos, 2017). Therefore, long-term increases in zinc
713 signaling, via Z-LTP, would enhance endocannabinoid activation during subsequent
714 stimulus trains, increase synaptic facilitation, and further enhance steady-state EPSCs.
715 Conversely, long-term decreases in zinc signaling, via Z-LTD, would reduce
716 endocannabinoid activation, decrease synaptic facilitation, and suppress steady-state
717 EPSCs.
718
719 Following stimulus trains, zinc-mediated endocannabinoid activation causes short-term
720 depression and inhibits short-term facilitation (Perez-Rosello *et al.*, 2013). Therefore, Z-
721 LTP and Z-LTD are expected to shift the balance between short-term facilitation and short-
722 term depression in DCN synapses. Z-LTP will enhance subsequent zinc-mediated short-
723 term depression, whereas Z-LTD will enhance short-term facilitation. Taken together, our
724 results highlight a powerful mechanism by which long-term bidirectional zinc plasticity may
725 modulate short-term glutamatergic synaptic plasticity.
726
727 **Implications of Z-LTP and Z-LTD for LTD and LTP.** In central synapses, including DCN
728 PF synapses, the direction and size of LTP or LTD are determined by the combination of
729 multiple simultaneous LTP and LTD mechanisms (O'Connor *et al.*, 2005; Bender *et al.*,
730 2006; Tzounopoulos *et al.*, 2007; Shen *et al.*, 2008; Zhao & Tzounopoulos, 2011). In DCN
731 PF synapses, LTP and LTD are influenced by the coactivation of pre- and postsynaptic
732 signaling mechanisms including NMDARs, mGluRs, muscarinic acetylcholine receptors,
733 and endocannabinoid signaling (Fujino & Oertel, 2003; Tzounopoulos *et al.*, 2007; Zhao &
734 Tzounopoulos, 2011). Therefore, bidirectional zinc plasticity likely acts together with these
735 other known mechanisms to shape the size and direction of synaptic plasticity.
736

737 Several of our results are consistent with this notion. As shown in Figure 2, blockade of
738 NMDARs did not block either HFS-induced LTP or Z-LTD. This indicates that NMDAR-
739 independent LTP was induced, suggesting that Z-LTD contributes to NMDAR-independent
740 LTP (Figure 2 A). G1 mGluR antagonists blocked HFS-induced Z-LTD (Figure 2 B).
741 Therefore, the induced LTP under these conditions is NMDAR-, G1 mGluR-, and Z-LTD-
742 independent. As shown in Figure 3 A, LFS induced Z-LTP; however, LFS did not induce
743 LTD. This suggests that LFS also induced an LTP that counterbalances the LTD effect of
744 Z-LTP. This is consistent with previous studies showing that LTP and LTD mechanisms
745 occur simultaneously in DCN PF synapses (Tzounopoulos *et al.*, 2007). G1 mGluR
746 antagonists blocked Z-LTP, but LTD was induced under these conditions (Figure 3 B),
747 suggesting that this LTD is NMDAR-, G1 mGluR-, and Z-LTP-independent. Taken
748 together, all these results are consistent with previous studies and further support the
749 notion that LTP and LTD are the result of coactivation of different signaling pathways of
750 long-term plasticity in the DCN (Fujino & Oertel, 2003; Tzounopoulos *et al.*, 2007; Zhao &
751 Tzounopoulos, 2011). Nevertheless, our results add Z-LTP and Z-LTD as new
752 mechanisms of LTD and LTP at zinc-containing glutamatergic synapses.
753
754 In DCN PFs, mGluR activation contributes to both HFS-induced LTP and LFS-induced
755 LTD (Fujino & Oertel, 2003). Our findings on HFS-induced LTP in CWCs are consistent
756 with Fujino & Oertel, 2003 (Fujino & Oertel, 2003), demonstrating mGluR- and NMDAR-
757 independent LTP (Figure 2 B). However, Fujino & Oertel showed LFS-induced NMDAR-
758 dependent LTD, whereas here we observed LFS-induced NMDAR-independent LTD
759 (Figure 3 B). This discrepancy could be explained by the use of different LFS induction
760 protocols (5 Hz for 3 min here, vs. 1 Hz for 5 min. paired with postsynaptic depolarization)
761 and extracellular solutions (4/4 mM Ca^{2+}/Mg^{2+} here, vs. 2.4/1.3 mM Ca^{2+}/Mg^{2+}).

762 In addition to DCN PF synapses, Z-LTP and Z-LTD may contribute to LTD and LTP in
763 other synaptic zinc-containing brain areas which express G1 mGluR-dependent LTD and
764 LTP, such as the hippocampus, amygdala, and striatum (Oliet *et al.*, 1997; Huber *et al.*,
765 2000; Gubellini *et al.*, 2003; Topolnik *et al.*, 2006; Wu *et al.*, 2008; Anwyl, 2009; Luscher &
766 Huber, 2010; Chen *et al.*, 2017; McAllister & Dyck, 2017). In the hippocampus, LFS
767 induces G1 mGluR-mediated LTD, whereas HFS induces LTP (Oliet *et al.*, 1997; Huber *et*
768 *al.*, 2000; Topolnik *et al.*, 2006; Wu *et al.*, 2008; Anwyl, 2009). Therefore, LFS-induced Z-
769 LTP would likely further enhance the effects of G1 mGluR-LTD, by increasing zinc
770 inhibition of AMPARs; whereas HFS-induced Z-LTD would further enhance the effects of
771 LTP, by reducing zinc inhibition of AMPARs. Thus, synaptic zinc plasticity likely serves as
772 a positive feedback mechanism to enhance the effects of G1 mGluR-dependent LTP or
773 LTD on glutamatergic synaptic transmission.
774
775 **Implications of Z-LTP and Z-LTD for metaplasticity.** Our results reveal that the
776 induction of Z-LTP and Z-LTD is NMDAR-independent. However, zinc inhibits NMDARs
777 and thus modulates the induction of NMDAR-dependent LTP and LTD in the hippocampus
778 (Izumi *et al.*, 2006; Takeda *et al.*, 2009; Vergnano *et al.*, 2014). As such, long-term
779 synaptic zinc plasticity may contribute to 'metaplasticity', the modulation of subsequent
780 LTP and LTD (Abraham & Tate, 1997). Z-LTD, by reducing the inhibitory effect of zinc on
781 NMDARs, may promote subsequent NMDAR-dependent LTP and decrease subsequent
782 NMDAR-dependent LTD. Conversely, Z-LTP, by enhancing the inhibitory effect of zinc on
783 NMDARs, may promote subsequent NMDAR-LTD over NMDAR-LTP. Therefore, zinc
784 plasticity likely serves as a positive feedback mechanism for NMDAR-dependent
785 metaplasticity.
786

787 Synaptic zinc contributes to mossy fiber presynaptic LTP in response to HFS, via
788 activation of TrkB receptors (Huang *et al.*, 2008; Pan *et al.*, 2011). Therefore, if HFS
789 induces Z-LTD in mossy fiber synapses, it would act as a negative feedback signal for
790 subsequent LTP induction. Taken together, we propose that the role of Z-LTD and Z-LTP
791 in LTP and LTD depends on the specific mechanisms underlying LTP and LTD, but
792 overall, Z-LTD and Z-LTP likely act as positive feedback signals in G1 mGluR-dependent
793 synaptic plasticity and NMDAR-dependent metaplasticity.
794
795 **Clinical and translational implications of zinc plasticity.** In the context of zinc plasticity
796 as a positive feedback signal for NMDAR-dependent metaplasticity, it is interesting that
797 exposure to loud sound – known to induce tinnitus – causes Z-LTD in the DCN. Although
798 not tested here, it is possible that Z-LTD could potentially lead to runaway excitation due to
799 enhanced LTP and decreased LTD, and thus to pathological DCN hyperactivity associated
800 with tinnitus (Tzounopoulos, 2008). Noise-induced pathological hyperexcitability through
801 LTP/LTD-like mechanisms in the DCN PF synapses has been hypothesized and recently
802 implicated in tinnitus treatment (Tzounopoulos, 2008; Marks *et al.*, 2018), therefore
803 suggesting that noise-induced reductions in synaptic zinc might contribute to tinnitus.
804
805 **References**

806 Abdul-Ghani MA, Valiante TA, Carlen PL & Pennefather PS. (1996). Metabotropic
807 glutamate receptors coupled to IP3 production mediate inhibition of IAHP in
808 rat dentate granule neurons. *J Neurophysiol* **76,** 2691-2700.
809
810 Abraham WC & Tate WP. (1997). Metaplasticity: a new vista across the field of
811 synaptic plasticity. *Prog Neurobiol* **52,** 303-323.
812
813 Anderson CT, Kumar M, Xiong S & Tzounopoulos T. (2017). Cell-specific gain
814 modulation by synaptically released zinc in cortical circuits of audition. *Elife* **6**.
815

816 Anderson CT, Radford RJ, Zastrow ML, Zhang DY, Apfel UP, Lippard SJ & Tzounopoulos
817 T. (2015). Modulation of extrasynaptic NMDA receptors by synaptic and tonic
818 zinc. *Proc Natl Acad Sci U S A* **112,** E2705-2714.
819
820 Anwyl R. (2009). Metabotropic glutamate receptor-dependent long-term potentiation.
821 *Neuropharmacology* **56,** 735-740.
822
823 Auerbach BD, Rodrigues PV & Salvi RJ. (2014). Central gain control in tinnitus and
824 hyperacusis. *Front Neurol* **5,** 206.
825
826 Bender VA, Bender KJ, Brasier DJ & Feldman DE. (2006). Two coincidence detectors
827 for spike timing-dependent plasticity in somatosensory cortex. *J Neurosci* **26,**
828 4166-4177.
829
830 Bilak SR & Morest DK. (1998). Differential expression of the metabotropic glutamate
831 receptor mGluR1alpha by neurons and axons in the cochlear nucleus: in situ
832 hybridization and immunohistochemistry. *Synapse* **28,** 251-270.
833
834 Brown CE & Dyck RH. (2002). Rapid, experience-dependent changes in levels of
835 synaptic zinc in primary somatosensory cortex of the adult mouse. *J Neurosci*
836 **22,** 2617-2625.
837
838 Brown CE & Dyck RH. (2005). Modulation of synaptic zinc in barrel cortex by whisker
839 stimulation. *Neuroscience* **134,** 355-359.
840
841 Chen A, Hu WW, Jiang XL, Potegal M & Li H. (2017). Molecular mechanisms of group I
842 metabotropic glutamate receptor mediated LTP and LTD in basolateral
843 amygdala in vitro. *Psychopharmacology (Berl)* **234,** 681-694.
844
845 Cole TB, Wenzel HJ, Kafer KE, Schwartzkroin PA & Palmiter RD. (1999). Elimination of
846 zinc from synaptic vesicles in the intact mouse brain by disruption of the ZnT3
847 gene. *Proc Natl Acad Sci U S A* **96,** 1716-1721.
848
849 Conn PJ & Pin JP. (1997). Pharmacology and functions of metabotropic glutamate
850 receptors. *Annu Rev Pharmacol Toxicol* **37,** 205-237.
851
852 Danscher G & Stoltenberg M. (2005). Zinc-specific autometallographic in vivo
853 selenium methods: tracing of zinc-enriched (ZEN) terminals, ZEN pathways,
854 and pools of zinc ions in a multitude of other ZEN cells. *J Histochem Cytochem*
855 **53,** 141-153.
856
857 Dyck RH, Chaudhuri A & Cynader MS. (2003). Experience-dependent regulation of the
858 zincergic innervation of visual cortex in adult monkeys. *Cereb Cortex* **13,** 1094-
859 1109.

860
861 Frederickson CJ, Howell GA, Haigh MD & Danscher G. (1988). Zinc-containing fiber
862 systems in the cochlear nuclei of the rat and mouse. *Hear Res* **36,** 203-211.
863
864 Frederickson CJ, Koh JY & Bush AI. (2005). The neurobiology of zinc in health and
865 disease. *Nat Rev Neurosci* **6,** 449-462.
866
867 Fujino K & Oertel D. (2003). Bidirectional synaptic plasticity in the cerebellum-like
868 mammalian dorsal cochlear nucleus. *Proc Natl Acad Sci U S A* **100,** 265-270.
869
870 Gubellini P, Saulle E, Centonze D, Costa C, Tropepi D, Bernardi G, Conquet F &
871 Calabresi P. (2003). Corticostriatal LTP requires combined mGluR1 and
872 mGluR5 activation. *Neuropharmacology* **44,** 8-16.
873
874 Hansen KB, Ogden KK, Yuan H & Traynelis SF. (2014). Distinct functional and
875 pharmacological properties of Triheteromeric GluN1/GluN2A/GluN2B NMDA
876 receptors. *Neuron* **81,** 1084-1096.
877
878 Holbro N, Grunditz A & Oertner TG. (2009). Differential distribution of endoplasmic
879 reticulum controls metabotropic signaling and plasticity at hippocampal
880 synapses. *Proc Natl Acad Sci U S A* **106,** 15055-15060.
881
882 Huang YZ, Pan E, Xiong ZQ & McNamara JO. (2008). Zinc-mediated transactivation of
883 TrkB potentiates the hippocampal mossy fiber-CA3 pyramid synapse. *Neuron*
884 **57,** 546-558.
885
886 Huber KM, Kayser MS & Bear MF. (2000). Role for rapid dendritic protein synthesis in
887 hippocampal mGluR-dependent long-term depression. *Science* **288,** 1254-
888 1257.
889
890 Huber KM, Roder JC & Bear MF. (2001). Chemical induction of mGluR5- and protein
891 synthesis--dependent long-term depression in hippocampal area CA1. *J*
892 *Neurophysiol* **86,** 321-325.
893
894 Izumi Y, Auberson YP & Zorumski CF. (2006). Zinc modulates bidirectional
895 hippocampal plasticity by effects on NMDA receptors. *J Neurosci* **26,** 7181-
896 7188.
897
898 Kalappa BI, Anderson CT, Goldberg JM, Lippard SJ & Tzounopoulos T. (2015). AMPA
899 receptor inhibition by synaptically released zinc. *Proc Natl Acad Sci U S A* **112,**
900 15749-15754.
901
902 Kalappa BI & Tzounopoulos T. (2017). Context-Dependent Modulation of Excitatory
903 Synaptic Strength by Synaptically Released Zinc. *eNeuro* **4**.

Kim CH, Lee J, Lee JY & Roche KW. (2008). Metabotropic glutamate receptors: phosphorylation and receptor signaling. *J Neurosci Res* **86,** 1-10.

Kujawa SG & Liberman MC. (2009). Adding insult to injury: cochlear nerve degeneration after "temporary" noise-induced hearing loss. *J Neurosci* **29,** 14077-14085.

Kumar M, Xiong S, Tzounopoulos T & Anderson CT. (2019). Fine Control of Sound Frequency Tuning and Frequency Discrimination Acuity by Synaptic Zinc Signaling in Mouse Auditory Cortex. *J Neurosci* **39,** 854-865.

Li Y, Andereggen L, Yuki K, Omura K, Yin Y, Gilbert HY, Erdogan B, Asdourian MS, Shrock C, de Lima S, Apfel UP, Zhuo Y, Hershfinkel M, Lippard SJ, Rosenberg PA & Benowitz L. (2017). Mobile zinc increases rapidly in the retina after optic nerve injury and regulates ganglion cell survival and optic nerve regeneration. *Proc Natl Acad Sci U S A* **114,** E209-E218.

Liguz-Lecznar M, Nowicka D, Czupryn A & Skangiel-Kramska J. (2005). Dissociation of synaptic zinc level and zinc transporter 3 expression during postnatal development and after sensory deprivation in the barrel cortex of mice. *Brain Res Bull* **66,** 106-113.

Luscher C & Huber KM. (2010). Group 1 mGluR-dependent synaptic long-term depression: mechanisms and implications for circuitry and disease. *Neuron* **65,** 445-459.

Malenka RC & Bear MF. (2004). LTP and LTD: an embarrassment of riches. *Neuron* **44,** 5-21.

Malenka RC & Nicoll RA. (1993). NMDA-receptor-dependent synaptic plasticity: multiple forms and mechanisms. *Trends Neurosci* **16,** 521-527.

Manis PB, Spirou GA, Wright DD, Paydar S & Ryugo DK. (1994). Physiology and morphology of complex spiking neurons in the guinea pig dorsal cochlear nucleus. *J Comp Neurol* **348,** 261-276.

Marks KL, Martel DT, Wu C, Basura GJ, Roberts LE, Schvartz-Leyzac KC & Shore SE. (2018). Auditory-somatosensory bimodal stimulation desynchronizes brain circuitry to reduce tinnitus in guinea pigs and humans. *Sci Transl Med* **10**.

McAllister BB & Dyck RH. (2017). Zinc transporter 3 (ZnT3) and vesicular zinc in central nervous system function. *Neurosci Biobehav Rev* **80,** 329-350.

948 Mulkey RM & Malenka RC. (1992). Mechanisms underlying induction of homosynaptic
949 long-term depression in area CA1 of the hippocampus. *Neuron* **9,** 967-975.
950
951 Nakashima AS, Butt RH & Dyck RH. (2011). Alterations in protein and gene expression
952 within the barrel cortices of ZnT3 knockout mice: experience-independent and
953 dependent changes. *Neurochem Int* **59,** 860-870.
954
955 Nakashima AS & Dyck RH. (2009). Zinc and cortical plasticity. *Brain Res Rev* **59,** 347-
956 373.
957
958 Nakashima AS & Dyck RH. (2010). Dynamic, experience-dependent modulation of
959 synaptic zinc within the excitatory synapses of the mouse barrel cortex.
960 *Neuroscience* **170,** 1015-1019.
961
962 O'Connor DH, Wittenberg GM & Wang SS. (2005). Dissection of bidirectional synaptic
963 plasticity into saturable unidirectional processes. *J Neurophysiol* **94,** 1565-
964 1573.
965
966 Oliet SH, Malenka RC & Nicoll RA. (1997). Two distinct forms of long-term depression
967 coexist in CA1 hippocampal pyramidal cells. *Neuron* **18,** 969-982.
968
969 Palmiter RD, Cole TB, Quaife CJ & Findley SD. (1996). ZnT-3, a putative transporter of
970 zinc into synaptic vesicles. *Proc Natl Acad Sci U S A* **93,** 14934-14939.
971
972 Pan E, Zhang XA, Huang Z, Krezel A, Zhao M, Tinberg CE, Lippard SJ & McNamara JO.
973 (2011). Vesicular zinc promotes presynaptic and inhibits postsynaptic long-
974 term potentiation of mossy fiber-CA3 synapse. *Neuron* **71,** 1116-1126.
975
976 Paoletti P, Ascher P & Neyton J. (1997). High-affinity zinc inhibition of NMDA NR1-
977 NR2A receptors. *J Neurosci* **17,** 5711-5725.
978
979 Perez-Rosello T, Anderson CT, Schopfer FJ, Zhao Y, Gilad D, Salvatore SR, Freeman BA,
980 Hershfinkel M, Aizenman E & Tzounopoulos T. (2013). Synaptic Zn2+ inhibits
981 neurotransmitter release by promoting endocannabinoid synthesis. *J Neurosci*
982 **33,** 9259-9272.
983
984 Pick JE & Ziff EB. (2018). Regulation of AMPA receptor trafficking and exit from the
985 endoplasmic reticulum. *Mol Cell Neurosci*.
986
987 Rachline J, Perin-Dureau F, Le Goff A, Neyton J & Paoletti P. (2005). The micromolar
988 zinc-binding domain on the NMDA receptor subunit NR2B. *J Neurosci* **25,** 308-
989 317.
990

991 Rubio ME & Juiz JM. (1998). Chemical anatomy of excitatory endings in the dorsal
992 cochlear nucleus of the rat: differential synaptic distribution of aspartate
993 aminotransferase, glutamate, and vesicular zinc. *J Comp Neurol* **399,** 341-358.
994
995 Ryugo DK & Willard FH. (1985). The dorsal cochlear nucleus of the mouse: a light
996 microscopic analysis of neurons that project to the inferior colliculus. *J Comp*
997 *Neurol* **242,** 381-396.
998
999 Salazar G, Craige B, Love R, Kalman D & Faundez V. (2005). Vglut1 and ZnT3 co-
1000 targeting mechanisms regulate vesicular zinc stores in PC12 cells. *J Cell Sci* **118,**
1001 1911-1921.
1002
1003 Shen W, Flajolet M, Greengard P & Surmeier DJ. (2008). Dichotomous dopaminergic
1004 control of striatal synaptic plasticity. *Science* **321,** 848-851.
1005
1006 Snyder EM, Philpot BD, Huber KM, Dong X, Fallon JR & Bear MF. (2001).
1007 Internalization of ionotropic glutamate receptors in response to mGluR
1008 activation. *Nat Neurosci* **4,** 1079-1085.
1009
1010 Suter BA, O'Connor T, Iyer V, Petreanu LT, Hooks BM, Kiritani T, Svoboda K &
1011 Shepherd GM. (2010). Ephus: multipurpose data acquisition software for
1012 neuroscience experiments. *Front Neural Circuits* **4,** 100.
1013
1014 Takeda A, Fuke S, Ando M & Oku N. (2009). Positive modulation of long-term
1015 potentiation at hippocampal CA1 synapses by low micromolar concentrations
1016 of zinc. *Neuroscience* **158,** 585-591.
1017
1018 Topolnik L, Azzi M, Morin F, Kougioumoutzakis A & Lacaille JC. (2006). mGluR1/5
1019 subtype-specific calcium signalling and induction of long-term potentiation in
1020 rat hippocampal oriens/alveus interneurones. *J Physiol* **575,** 115-131.
1021
1022 Tovar KR & Westbrook GL. (2012). Amino-terminal ligands prolong NMDA Receptor-
1023 mediated EPSCs. *J Neurosci* **32,** 8065-8073.
1024
1025 Traynelis SF, Wollmuth LP, McBain CJ, Menniti FS, Vance KM, Ogden KK, Hansen KB,
1026 Yuan H, Myers SJ & Dingledine R. (2010). Glutamate receptor ion channels:
1027 structure, regulation, and function. *Pharmacol Rev* **62,** 405-496.
1028
1029 Tzounopoulos T. (2008). Mechanisms of synaptic plasticity in the dorsal cochlear
1030 nucleus: plasticity-induced changes that could underlie tinnitus. *Am J Audiol*
1031 **17,** S170-175.
1032
1033 Tzounopoulos T, Kim Y, Oertel D & Trussell LO. (2004). Cell-specific, spike timing-
1034 dependent plasticities in the dorsal cochlear nucleus. *Nat Neurosci* **7,** 719-725.

1035
1036 Tzounopoulos T, Rubio ME, Keen JE & Trussell LO. (2007). Coactivation of pre- and
1037 postsynaptic signaling mechanisms determines cell-specific spike-timing-
1038 dependent plasticity. *Neuron* **54,** 291-301.
1039
1040 Vergnano AM, Rebola N, Savtchenko LP, Pinheiro PS, Casado M, Kieffer BL, Rusakov
1041 DA, Mulle C & Paoletti P. (2014). Zinc dynamics and action at excitatory
1042 synapses. *Neuron* **82,** 1101-1114.
1043
1044 Vogt K, Mellor J, Tong G & Nicoll R. (2000). The actions of synaptically released zinc at
1045 hippocampal mossy fiber synapses. *Neuron* **26,** 187-196.
1046
1047 Wisniewski K & Car H. (2002). (S)-3,5-DHPG: a review. *CNS Drug Rev* **8,** 101-116.
1048
1049 Wright DD, Blackstone CD, Huganir RL & Ryugo DK. (1996). Immunocytochemical
1050 localization of the mGluR1 alpha metabotropic glutamate receptor in the dorsal
1051 cochlear nucleus. *J Comp Neurol* **364,** 729-745.
1052
1053 Wu J, Harney S, Rowan MJ & Anwyl R. (2008). Involvement of group I mGluRs in LTP
1054 induced by strong high frequency stimulation in the dentate gyrus in vitro.
1055 *Neurosci Lett* **436,** 235-238.
1056
1057 Zastrow ML, Radford RJ, Chyan W, Anderson CT, Zhang DY, Loas A, Tzounopoulos T &
1058 Lippard SJ. (2016). Reaction-Based Probes for Imaging Mobile Zinc in Live Cells
1059 and Tissues. *ACS Sens* **1,** 32-39.
1060
1061 Zhang S & Oertel D. (1993). Cartwheel and superficial stellate cells of the dorsal
1062 cochlear nucleus of mice: intracellular recordings in slices. *J Neurophysiol* **69,**
1063 1384-1397.
1064
1065 Zhao Y & Tzounopoulos T. (2011). Physiological activation of cholinergic inputs
1066 controls associative synaptic plasticity via modulation of endocannabinoid
1067 signaling. *J Neurosci* **31,** 3158-3168.
1068
1069 Zhou J, Nannapaneni N & Shore S. (2007). Vessicular glutamate transporters 1 and 2
1070 are differentially associated with auditory nerve and spinal trigeminal inputs
1071 to the cochlear nucleus. *J Comp Neurol* **500,** 777-787.
1072
1073
1074
1075

1076 **Figure Legends**

1077 **Figure 1. High-frequency stimulation (HFS) induces Z-LTD in DCN parallel fiber**
1078 **synapses. (A)** Schematic of experimental setup illustrating stimulation of zinc-rich
1079 glutamatergic DCN parallel fibers (PFs) and whole-cell recording of a postsynaptic
1080 cartwheel cell (CWC). **(B)** *Left:* Time course of AMPAR EPSC amplitude before and after
1081 ZX1 application, normalized to baseline before ZX1 application (100 μM). *Right:* Example
1082 AMPAR EPSCs before and after ZX1 application, showing ZX1 potentiation. **(C)** *Left:* Time
1083 course of AMPAR EPSC amplitude before and after HFS, and before and after subsequent
1084 ZX1 application (blue). After obtaining a stable baseline, HFS was delivered (3 x 100 Hz
1085 for 1 sec, 10 sec ISI). EPSC % baseline after HFS (mins. 19-23): n=11, *p=0.041, one-
1086 sample t test vs. 100%. Star (*) indicates significant LTP. To examine ZX1 potentiation
1087 after HFS, after obtaining a stable baseline after HFS, AMPAR EPSC amplitude was
1088 renormalized to the new baseline before ZX1 application. The renormalization is indicated
1089 by a gap and restart of timing in the x-axis. For comparison, red line shows normalized
1090 time course of AMPAR EPSC amplitude before and after ZX1 application in controls
1091 replotted from **B**. *Right:* Example AMPAR EPSCs showing no ZX1 potentiation after HFS.
1092 **(D)** Average ZX1 potentiation (% increase from baseline) during the last 5 min of ZX1
1093 application. 'Control' (n=10) vs. 'HFS' (n=11): *p=0.002, unpaired t test. The reduction in
1094 ZX1 potentiation is termed Z-LTD. Values represent mean ± SEM. Star (*) indicates
1095 p<0.05. For detailed values and statistical tests for all figures, see Materials and Methods,
1096 Statistical Analysis section.

1097

1098 **Figure 2. Group 1 mGluR activation is required for HFS-induced Z-LTD. (A)** Time
1099 course of AMPAR EPSC amplitude before and after HFS in the presence of APV (50 μM),

1100 and before and after subsequent ZX1 application. EPSC % baseline after HFS (mins. 19-
1101 23): n=9, *p=0.0008, one-sample t test vs. 100%. **(B)** Same time course as in **A** but in the
1102 presence of LY367385 (100 μM), MPEP (4 μM), and APV (50 μM). EPSC % baseline after
1103 HFS (mins. 19-23): n=6, *p=0.041, one-sample t test vs. 100%. For **(A-B)**, star (*) indicates
1104 significant LTP. To examine ZX1 potentiation after HFS, similar approach and
1105 renormalization as in **1C** was performed. Red line shows the time course of AMPAR EPSC
1106 amplitude before and after ZX1 application in control replotted from **1B**. Example traces
1107 show AMPAR EPSCs before and after ZX1. **(C)** Average ZX1 potentiation (% increase
1108 from baseline) during the last 5 min of ZX1 application, with control data from **1D.** 'HFS +
1109 APV' (n=9) reduced ZX1 potentiation compared to control; this reduction was blocked by
1110 LY367385 and MPEP (n=5). One-way ANOVA/Bonferroni, *p=0.003. Values represent
1111 mean ± SEM. Star (*) indicates p<0.05.
1112
1113 **Figure 3. Low frequency stimulation (LFS) induces Z-LTP, which requires Group 1**
1114 **mGluR activation. (A)** Time course of AMPAR EPSC amplitude before and after LFS (5
1115 Hz, 3 min), and before and after subsequent ZX1 application (cyan); and similar time
1116 course in interleaved control experiments (without LFS, red). **(B)** Same time course as in **A**
1117 but in the presence of LY367385 (100 μM) and MPEP (4 μM) (green). EPSC % baseline
1118 after LFS (mins. 20-24): n=6, *p=0.006, one-sample t test vs. 100%. Star (*) indicates
1119 significant LTD. Red line shows similar time course in controls replotted from **A**. For **(A-B)**,
1120 to examine the ZX1 potentiation after LFS, similar approach and renormalization as in **1C**
1121 was performed. Example traces show AMPAR EPSCs before and after ZX1. **(C)** Average
1122 ZX1 potentiation (% increase from baseline) during the last 5 min of ZX1 application.
1123 'Control': n=5; 'LFS': n=6; 'LFS + LY367385, MPEP': n=6. LFS increased ZX1 potentiation

1124 compared to control; this increase was blocked by LY367385 and MPEP. One-way
1125 ANOVA/Bonferroni, *p=0.02. The increase in ZX1 potentiation is termed Z-LTP. Values
1126 represent mean ± SEM. Star (*) indicates p<0.05.
1127
1128 **Figure 4. Group 1 mGluR activation is sufficient to induce Z-LTP and Z-LTD. (A)** Time
1129 course of AMPAR EPSC amplitude before and after application of 50 μM DHPG, and
1130 before and after subsequent ZX1 application. EPSC % baseline after 50 μM DHPG (mins.
1131 16-20): n=6, *p=0.0002, one-sample t test vs. 100%. Star (*) indicates significant synaptic
1132 depression. **(B)** Time course of AMPAR EPSC amplitude before and after application of 5
1133 μM DHPG, and before and after subsequent ZX1 application. For **(A-B)**, to examine the
1134 ZX1 potentiation after DHPG application, after obtaining a stable baseline after DHPG,
1135 AMPAR EPSC amplitude was renormalized to the new baseline before ZX1 application.
1136 The renormalization is indicated by a gap and restart of timing in the x-axis. Example
1137 traces show AMPAR EPSCs before and after ZX1. **(C)** Average ZX1 potentiation (%
1138 increase from baseline) during the last 5 min of ZX1 application, with control data from **1D**.
1139 'DHPG (50 μM)': n=5; 'DHPG (5 μM)': n=5. DHPG (50 μM) increased ZX1 potentiation
1140 compared to control, whereas DHPG (5 μM) reduced ZX1 potentiation compared to
1141 control. One-way ANOVA/Bonferroni, *p<0.0001. Increased and decreased ZX1
1142 potentiation correspond to Z-LTP and Z-LTD, respectively. **(D)** Similar time course as in **A**,
1143 but in same extracellular conditions as in **3A-B**. EPSC % baseline after 50 μM DHPG
1144 (mins. 16-20): n=5, *p=0.044, one-sample t test vs. 100%. Star (*) indicates significant
1145 synaptic depression. **(E)** Time course of AMPAR EPSC amplitude before and after
1146 sequential LFS (5 Hz, 3 min) and application of 50 μM DHPG, and before and after
1147 subsequent ZX1 application, in same conditions as in **D**. For **(D-E)**, to examine the ZX1

1148 potentiation, similar approach and renormalization as in **A-B** was performed. Example
1149 traces show AMPAR EPSCs before and after ZX1. **(F)** Average ZX1 potentiation (%
1150 increase from baseline) during the last 5 min of ZX1 application for the experiments in **D-E**,
1151 with LFS data from **3C**. 'DHPG (50 μM)': n=5; 'LFS + DHPG (50 μM)': n=5. Sequential LFS
1152 and DHPG (50 μM) did not increase ZX1 potentiation compared to LFS or DHPG (50 μM)
1153 alone. One-way ANOVA/Bonferroni: n.s. p=0.67. Values represent mean ± SEM. Star (*)
1154 indicates p<0.05.
1155
1156 **Figure 5. Group 1 mGluR activation bidirectionally modulates presynaptic zinc**
1157 **levels. (A)** *Left:* Schematic of the DCN, showing the presynaptic zinc-containing region,
1158 and the zinc-free region. *Right:* 20x image of DA-ZP1 fluorescence, demonstrating the
1159 zinc-containing ROI (zinc ROI) and the zinc-free ROI, before and after application of 50 μM
1160 DHPG. **(B)** Same approach as in **A**, before and after application of 5 μM DHPG. **(C)**
1161 Average DA-ZP1 fluorescence after application of 50 μM or 5 μM DHPG, normalized to
1162 baseline fluorescence before DHPG application. '+ DHPG (50 μM)': n=9, *p=0.004,
1163 Wilcoxon signed rank test vs. 100%. '+ DHPG (5 μM)': n=8, *p=0.008, Wilcoxon signed
1164 rank test vs. 100%. Values represent mean ± SEM. Star (*) indicates p<0.05.
1165
1166 **Figure 6. Group 1 mGluR-dependent Z-LTD reduces zinc inhibition of NMDARs. (A)**
1167 *Left:* Time course of AMPAR EPSC amplitude before and after HFS, and NMDAR EPSC
1168 amplitude before and after subsequent ZX1 application (blue); and similar time course in
1169 interleaved control experiments (without HFS, red). *Right:* Example NMDAR EPSCs before
1170 and after ZX1 application. **(B)** *Left:* Same time course as in **A** but in the presence of
1171 LY367385 (100 μM) and MPEP (4 μM) (green). Red line shows controls replotted from **A**.

1172 *Right:* Example NMDAR EPSCs before and after ZX1 application. For **(A-B)**, after
1173 obtaining a stable baseline of AMPAR EPSCs, HFS was delivered, then DNQX (20 μM)
1174 was applied. NMDAR EPSCs were then recorded at +40 mV normalized to the baseline
1175 NMDAR EPSC amplitude before ZX1 application. The switch from AMPAR to NMDAR
1176 EPSC time course, and the renormalization of EPSC amplitude are indicated by a gap and
1177 restart of timing in the x-axis. **(C)** Average ZX1 potentiation (% increase from baseline)
1178 during the last 5 min of ZX1 application. 'Control': n=5; 'HFS': n=6; 'HFS + LY367385,
1179 MPEP': n=5. HFS reduced ZX1 potentiation compared to control; this reduction was
1180 blocked by LY367385 and MPEP. Kruskal-Wallis test/Dunn: *p=0.01. **(D)** Dose-response
1181 of NMDAR EPSCs (% baseline) for increasing concentrations of ifenprodil, in controls (red)
1182 and after HFS (blue). 'Control': n=3-5 per concentration; 'HFS': n=3-4 per concentration.
1183 **(E)** IC_{50} of ifenprodil, from dose-responses in **D**. n.s. p=0.97, comparison of fits, extra sum-
1184 of-squares F test. Values represent mean ± SEM. Star (*) indicates p<0.05.
1185
1186 **Figure 7. Sound-induced Z-LTD requires Group 1 mGluR activation. (A)** Time course
1187 of AMPAR EPSC amplitude before and after ZX1 application in slices from N.E. mice
1188 (gray) and N.E. AIDA-treated mice (orange). Example traces show AMPAR EPSCs before
1189 and after ZX1. **(B)** Average ZX1 potentiation (% increase from baseline) during the last 5
1190 min of ZX1 application. 'N.E.' (n=5) vs. 'N.E. + AIDA' (n=6): *p=0.024, unpaired t test. **(C)**
1191 *Left:* Average paired-pulse ratio (PPR, pulse 2 / pulse 1) of baseline AMPAR EPSCs in
1192 slices from N.E. mice and N.E. AIDA-treated mice. 'N.E.' (n=5) vs. 'N.E. + AIDA' (n=6): n.s.
1193 p=0.476, unpaired t test. Example traces show AMPAR EPSCs in response to two pulses.
1194 *Right:* coefficient of variation (CV) analysis ($1/CV^2$) of baseline AMPAR EPSCs (pulse 1) in
1195 slices from N.E. mice and N.E. AIDA-treated mice, normalized to N.E. mice. 'N.E. + AIDA':

1196 n=6; n.s. p=0.44, Wilcoxon signed rank test vs. 1. **(D)** Example Auditory Brainstem
1197 Responses (ABRs, 10-80 dB SPL sound stimuli) from sham-exposed mice (recorded from
1198 sham-exposed, ipsilateral ear, black), N.E. mice (gray), and N.E. AIDA-treated mice
1199 (orange). Because no ABRs were detected in the ipsilateral ears of N.E. mice, ABRs were
1200 measured from ears contralateral to noise exposure. **(E)** *Left:* Average ABR thresholds (dB
1201 SPL). 'Sham ipsi.': n=8; 'N.E. contra.': n=6; 'N.E. + AIDA contra.': n=7. N.E. increased ABR
1202 thresholds compared to sham-exposed (*p=0.0002), but AIDA and N.E. did not affect
1203 increases in ABR thresholds compared to N.E. alone, Kruskal-Wallis test/Dunn. *Right:*
1204 Average ABR Wave I amplitude (μV). 'Sham ipsi.': n=8; 'N.E. contra.': n=6; 'N.E. + AIDA
1205 contra.': n=7. N.E. decreased ABR Wave I amplitude compared to sham-exposed
1206 (*p=0.0024), but AIDA and N.E. did not affect decreases in ABR Wave I amplitude
1207 compared to N.E. alone, Kruskal-Wallis test/Dunn. Values represent mean ± SEM. Star (*)
1208 indicates p<0.05.

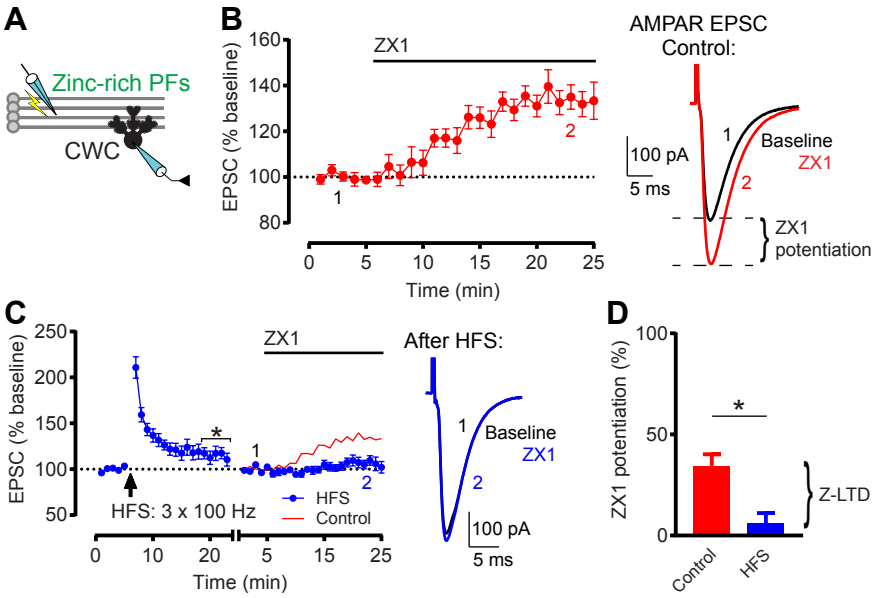
A
Zinc-rich PFs
CWC
B
ZX1
EPSC (% baseline)
160
140
120
100
80
1
2
0
5
10
15
20
25
Time (min)
AMPAR EPSC
Control:
100 pA
5 ms
1
2
Baseline
ZX1
ZX1
potentiation
C
ZX1
EPSC (% baseline)
250
200
150
100
50
*
1
2
HFS: 3 x 100 Hz
HFS
Control
0
10
20
5
15
25
Time (min)
After HFS:
1
2
Baseline
ZX1
100 pA
5 ms
D
ZX1 potentiation (%)
100
50
0
*
Z-LTD
Control
HFS

Figure 1

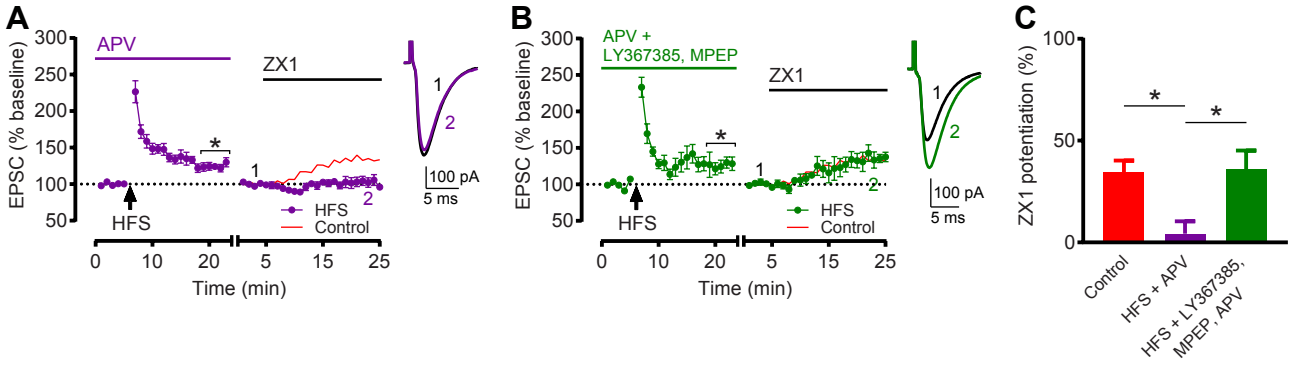
A
APV
ZX1
EPSC (% baseline)
300
250
200
150
100
50
HFS
HFS
Control
0
10
20
5
15
25
Time (min)
1
2
100 pA
5 ms
B
APV +
LY367385, MPEP
ZX1
EPSC (% baseline)
HFS
HFS
Control
Time (min)
1
2
100 pA
5 ms
C
ZX1 potentiation (%)
100
50
0
Control
HFS + APV
HFS + LY367385,
MPEP, APV

Figure 2

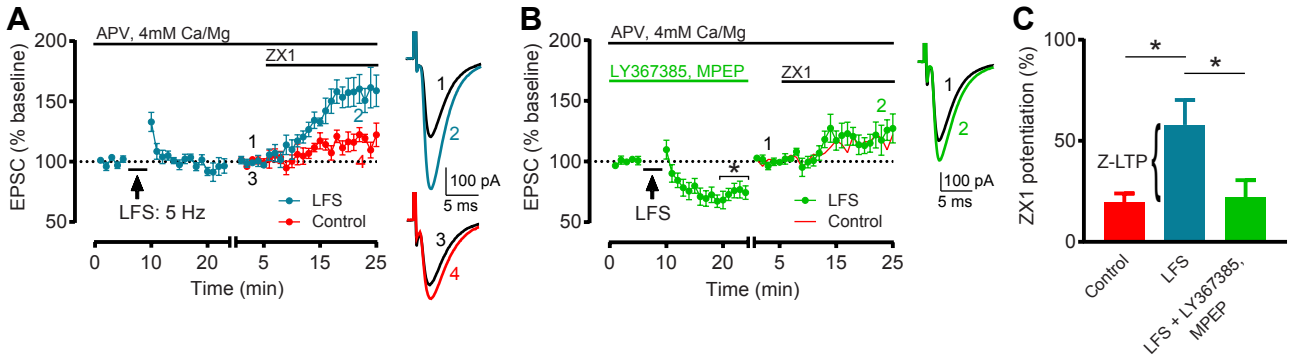
A
APV, 4mM Ca/Mg
ZX1
EPSC (% baseline)
200
150
100
50
LFS: 5 Hz
LFS
Control
0
10
20
5
15
25
Time (min)
1
2
3
4
100 pA
5 ms
B
APV, 4mM Ca/Mg
LY367385, MPEP
ZX1
EPSC (% baseline)
200
150
100
50
LFS
LFS
Control
0
10
20
5
15
25
Time (min)
*
1
2
100 pA
5 ms
C
ZX1 potentiation (%)
100
50
0
Z-LTP
*
*
Control
LFS
LFS + LY367385, MPEP

Figure 3

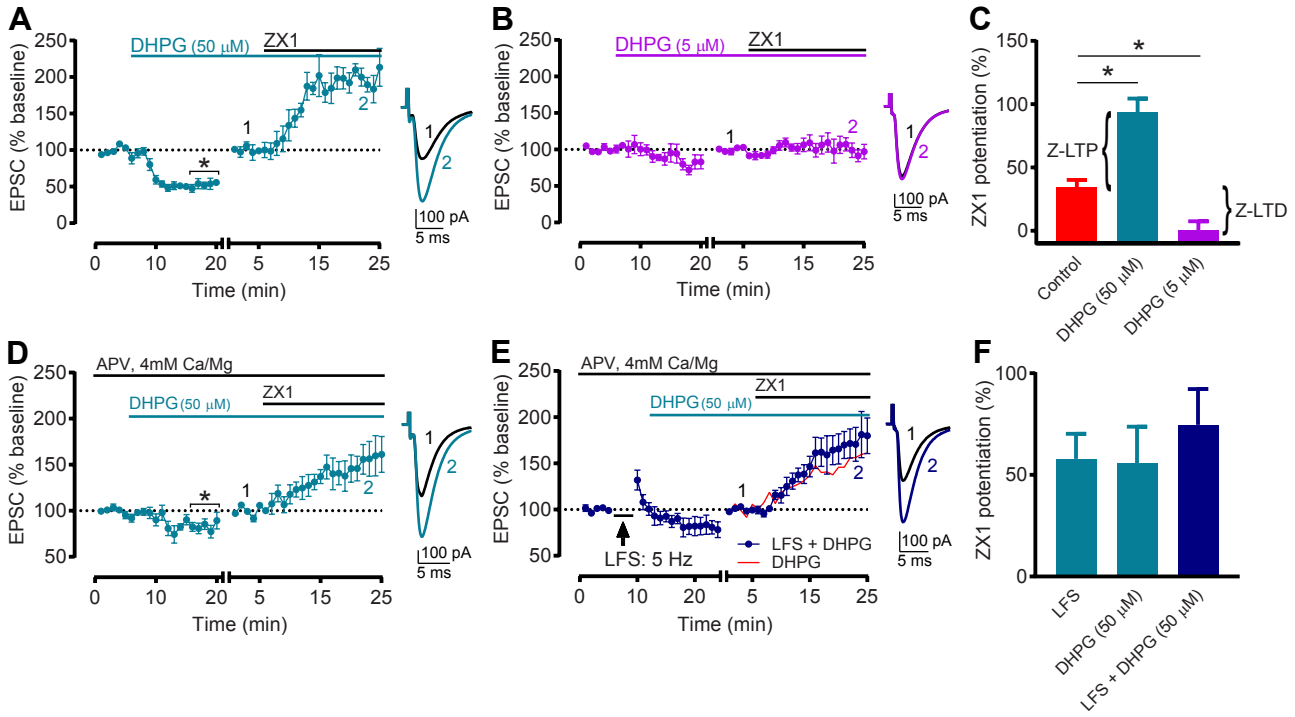
A
DHPG (50 μM)
ZX1
EPSC (% baseline)
Time (min)
100 pA
5 ms
B
DHPG (5 μM)
C
ZX1 potentiation (%)
Z-LTP
Z-LTD
Control
DHPG (50 μM)
DHPG (5 μM)
D
APV, 4mM Ca/Mg
E
LFS: 5 Hz
LFS + DHPG
DHPG
F
LFS
LFS + DHPG (50 μM)

Figure 4

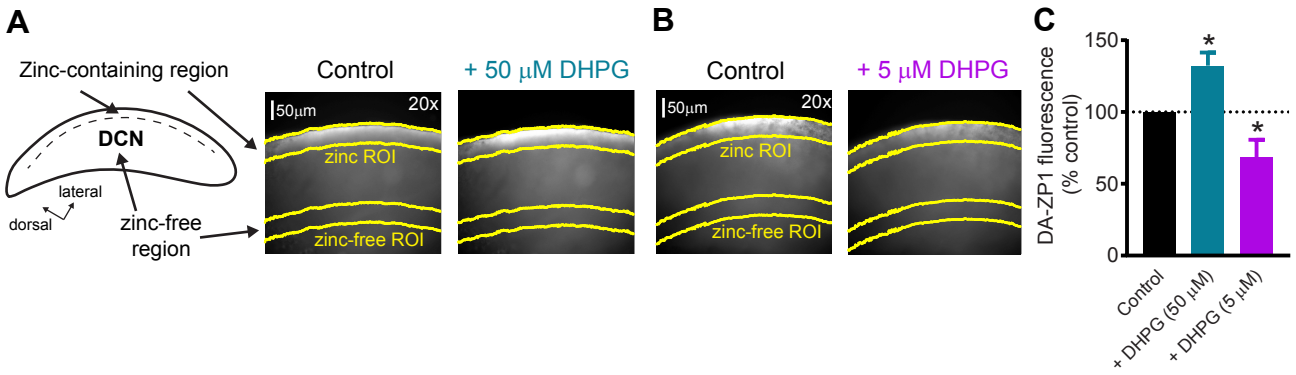
A
Zinc-containing region
DCN
lateral
dorsal
zinc-free region
Control
+ 50 μM DHPG
50μm
20x
zinc ROI
zinc-free ROI
B
Control
+ 5 μM DHPG
50μm
20x
zinc ROI
zinc-free ROI
C
DA-ZP1 fluorescence (% control)
150
100
50
0
*
*
Control
+ DHPG (50 μM)
+ DHPG (5 μM)

Figure 5

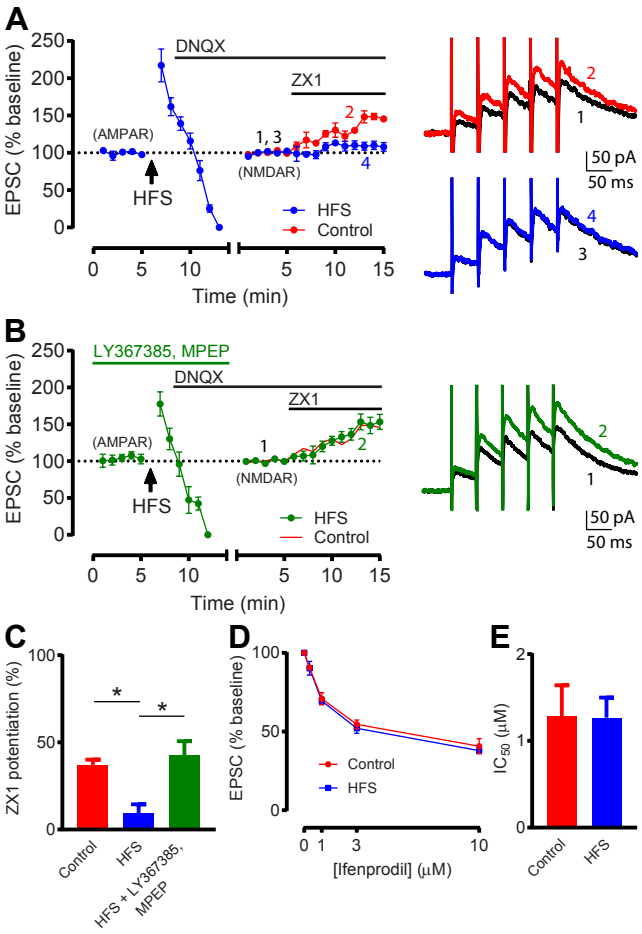
A
EPSC (% baseline)
250
200
150
100
50
0
DNQX
ZX1
(AMPAR)
HFS
1, 3
(NMDAR)
2
4
HFS
Control
0
5
10
5
10
15
Time (min)
1
2
3
4
50 pA
50 ms
B
LY367385, MPEP
DNQX
ZX1
(AMPAR)
HFS
1
(NMDAR)
2
HFS
Control
Time (min)
C
ZX1 potentiation (%)
100
50
0
*
*
Control
HFS
HFS + LY367385, MPEP
D
EPSC (% baseline)
Control
HFS
0
1
3
10
[Ifenprodil] (μM)
E
IC50 (μM)
2
1
0
Control
HFS

Figure 6

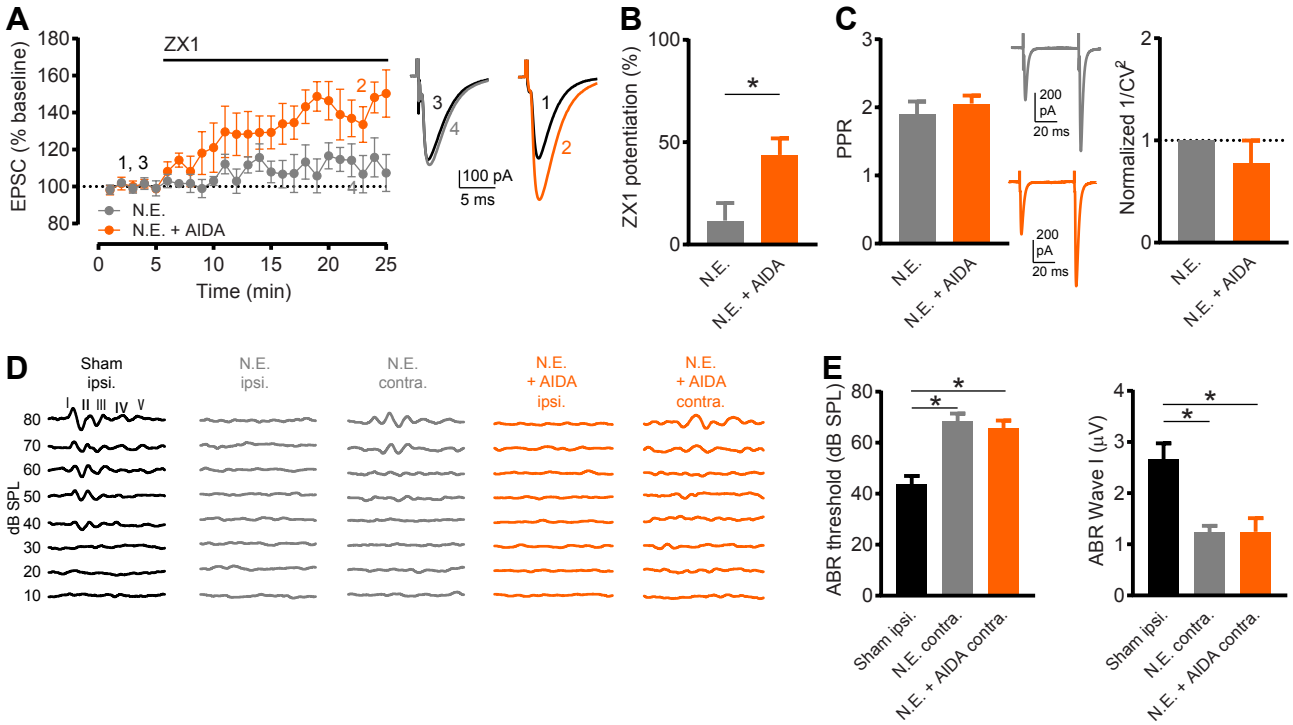
A
EPSC (% baseline)
ZX1
1, 3
2
N.E.
N.E. + AIDA
Time (min)
3
4
1
2
100 pA
5 ms
B
ZX1 potentiation (%)
*
N.E.
N.E. + AIDA
C
PPR
200 pA
20 ms
Normalized 1/CV²
D
Sham ipsi.
N.E. ipsi.
N.E. contra.
N.E. + AIDA ipsi.
N.E. + AIDA contra.
dB SPL
E
ABR threshold (dB SPL)
ABR Wave I (μV)
Sham ipsi.
N.E. contra.
N.E. + AIDA contra.

Figure 7